2014

Tracing Archaean terranes under Greenland's Icecap: U-Th-Pb-Hf isotopic study of zircons from melt-water rivers in the Isua area

Keewook Yi
Korea Institute of Geoscience and Mineral Resources

Vickie Bennett
Australian National University, vickie.bennett@anu.edu.au

Allen Phillip Nutman
University of Wollongong, anutman@uow.edu.au

Seung Ryeol Lee
Korea Institute of Geoscience and Mineral Resources

Publication Details

Yi, K., Bennett, V. C., Nutman, A. P. & Lee, S. (2014). Tracing Archaean terranes under Greenland's Icecap: U-Th-Pb-Hf isotopic study of zircons from melt-water rivers in the Isua area. Precambrian Research, 255 (Part 3), 900-921.

Tracing Archaean terranes under Greenland's Icecap: U-Th-Pb-Hf isotopic study of zircons from melt-water rivers in the Isua area

Abstract

The Archaean gneisses of the Nuuk area (southern West Greenland) are partitioned into tectonostratigraphic terranes - blocks of arc-like crust that evolved independently until they coalesced by collisional orogeny. To 'map' terranes to the east under the Inland Ice, sand samples were taken from rivers issuing from the edge of the Icecap; three from the Isua area and one from ~20 km to the south. Bedrock along this part of the ice front consists of ~3820-3600 Ma amphibolite facies rocks. 40 km south of Isua (Kapisilik terrane in the Ivisaartoq area) and also from ~10 km to the north there are Mesoarchaean amphibolite facies gneisses (3070-2950 Ma) exposed at the ice front. In the moraine fields in the Isua area there are erratic blocks of granulite facies gneisses. These were sourced from a hidden terrane to the east under the ice because no such rocks are exposed in the Isua area. The majority of the zircons from the sand samples yielded close to concordant U-Pb ages. Apart from one 2414 Ma grain, all are Archaean. The Isua sands show ~2695, 2710 and 2730 Ma; then 2790, 2805 and 2840 Ma clusters with a few grains back to 2950 Ma and then a complex 3440-3960 Ma spectrum. Less than 1% of the grains have ages between 3000 and 3400 Ma. In the Isua sands, Neoarchaean and late Mesoarchaean zircons form >50% of the population. The sand 20 km to the south shows a similar span of zircon ages, but there is a 2960 Ma peak not seen in the Isua sands. As the Eoarchaean and late Mesoarchaean-Neoarchaean cycles progress, the spread of Th/U and εHf values seen in each zircon age population increases. This is interpreted as repeated addition of juvenile material to the crust, but also with increasing amounts of high temperature tectonothermal recycling of older materials within a package. However, there is no isotopic evidence for any contribution of Eoarchaean crust to the later ≥2750 Ma Archaean cycle(s), showing evolution in disparate terranes. Furthermore, no evidence for Hadean material beneath the ice is seen in either the U-Pb ages or Hf isotopic compositions of the detrital zircons. On the other hand, 2750-2500 Ma metamorphic zircons show a spread of initial εHf values of zero to −25, with the most negative indicating zircon growth in Eoarchaean rocks. Overall these results closely mirror those obtained from direct sampling of rocks of the Archaean terranes exposed beyond the Icecap. The zircon data indicate that Mesoarchaean rocks equivalent to the Kapisilik terrane are absent under the ice. Instead, zircons were sourced from a late Mesoarchaean to Neoarchaean terrane affected by high grade metamorphism, whose age spectra perfectly matches the Tasiusarsuaq terrane to the southeast of Nuuk. Guided by the zircon results and aeromagnetic signatures, a terrane map is presented that extrapolates the Tasiusarsuaq terrane northwards under the Inland Ice towards the Tuno terrane in the north of the craton. Implications for different syntheses on the evolution of Archaean crust in southern West Greenland are discussed.

Disciplines

Medicine and Health Sciences | Social and Behavioral Sciences

Publication Details

Yi, K., Bennett, V. C., Nutman, A. P. & Lee, S. (2014). Tracing Archaean terranes under Greenland's Icecap: U-Th-Pb-Hf isotopic study of zircons from melt-water rivers in the Isua area. Precambrian Research, 255 (Part 3), 900-921.

Tracing Archaean terranes under Greenland's Icecap: U-Th-Pb-Hf isotopic study of zircons from melt-water rivers in the Isua area

Keewook Yi[1], Vickie C. Bennett[2], Allen P. Nutman[3], Seung Ryeol Lee[4]

Precambrian Research v. 255, p. 900-921 (2014)

1 Korean Basic Science Institute, Daejeon 305-350, Korea

2 Research School of Earth Sciences, The Australian National University, Canberra, ACT 0200, Australia

3 GeoQuEST Research Centre, School of Earth & Environmental Sciences, University of Wollongong, Wollongong, NSW 2522, Australia

4 Korea Institute of Geoscience and Mineral Resources, Daejeon 305-350, Korea

Email contact: anutman@uow.edu.au

Abstract

The Archaean gneisses of the Nuuk area (southern West Greenland) are partitioned into tectonostratigraphic terranes – blocks of arc-like crust that evolved independently until they coalesced by collisional orogeny. To 'map' terranes to the east under the Inland Ice, sand samples were taken from rivers issuing from the edge of the Icecap; three from the Isua area and one from ~20 km to the south. Bedrock along this part of the ice front consists of ~3820-3600 Ma amphibolite facies rocks. 40 km south of Isua (Kapisilik terrane in the Ivisaartoq area) and also from ~10 km to the north there are Mesoarchaean amphibolite facies gneisses (3070-2950 Ma) exposed at the ice front. In the moraine fields in the Isua area there are erratic blocks of granulite facies gneisses. These were sourced from a hidden terrane to the east under the ice because no such rocks are exposed in the Isua area.

The majority of the zircons from the sand samples yielded close to concordant U-Pb ages. Apart from one 2414 Ma grain, all are Archaean. The Isua sands show ~2695, 2710 and 2730 Ma; then 2790, 2805 and 2840 Ma clusters with a few grains back to 2950 Ma and then a complex 3440-3960 Ma spectrum. Less than 1% of the grains have ages between 3000 and 3400 Ma. In the Isua sands, Neoarchaean and late Mesoarchaean zircons form >50% of the population. The sand 20 km to the south shows a similar span of zircon ages, but there is a 2960 Ma peak not seen in the Isua sands.

As the Eoarchaean and late Mesoarchaean-Neoarchaean cycles progress, the spread of Th/U and ε_{Hf} values seen in each zircon age population increases. This is interpreted as repeated addition of juvenile material to the crust, but also with increasing amounts of high temperature tectonothermal recycling of older materials within a package. However, there is no isotopic evidence for any contribution of Eoarchaean crust to the later $\geqslant$2750 Ma Archaean cycle(s), showing evolution in disparate terranes. Furthermore, no evidence for Hadean material beneath the ice is seen in either the U-Pb ages or Hf isotopic compositions of the detrital zircons. On the other hand, 2750-2500 Ma metamorphic zircons show a spread of initial ε_{Hf} values of zero to -25, with the most negative indicating zircon growth in Eoarchaean rocks.

Overall these results closely mirror those obtained from direct sampling of rocks of the Archaean terranes exposed beyond the Icecap.

The zircon data indicate that Mesoarchaean rocks equivalent to the Kapisilik terrane are absent under the ice. Instead, zircons were sourced from a late Mesoarchaean to Neoarchaean terrane affected by high grade metamorphism, whose age spectra perfectly matches the Tasiusarsuaq terrane to the southeast of Nuuk. Guided by the zircon results and aeromagnetic signatures, a terrane map is presented that extrapolates the Tasiusarsuaq terrane northwards under the Inland Ice towards the Tuno terrane in the north of the craton. Implications for different syntheses on the evolution of Archaean crust in southern West Greenland are discussed. (498)

Keywords: Isua; glacial sediments; Greenland Icecap; zircons; Hf isotopes; Archaean terranes

1. **Introduction**

Much of Greenland's geology is blanketed by the Inland Ice – causing difficulties in linking the geology on the east and west coasts and also more locally along the ice margins. The distribution of Precambrian terranes of different ages has been assessed by aeromagnetic signatures (e.g., Rasmussen and Thorning, 1999; Rasmussen and van Gool, 2000), plus a limited geochronological program from the GISP2 borehole (72°35'N 38°27'W) revealed direct age constraints (Nutman and Kalsbeek, unpublished U-Pb zircon analyses; Weis et al., 1997, whole rock Rb-Sr, Sm-Nd and Pb-Pb analyses). This provides the broadest-scale information, such as the disposition of major Palaeoproterozoic belts versus blocks of cratonic Archaean crust. Further information can be obtained from material that has been derived from under the ice cap. For example in West Greenland near the ice margin in the study area there are rare erratic blocks of low pressure granulite facies rocks (C.R.L. Friend and A.P. Nutman, unpublished field observations), where no such rocks are exposed. In this paper we present U-Th-Pb-Hf isotopic data for zircons from rivers issuing from the ice-front, to assess the geology hidden under the ice east of the Isua supracrustal belt and the adjacent metagranitoid and gneiss complex (Fig. 1). This area is important because it forms the world's best-preserved sample of early terrestrial crust (e.g., Nutman et al., 2013a,b and references therein). Specific objectives were to determine (i) the distribution of Eoarchaean (~3800 and ~3700 Ma) terranes under the icecap, (ii) discern if there are rocks significantly older than the 3820-3600 Ma ones exposed along this part of the ice front, and (iii) whether the Mesoarchaean Kapisilik terrane (Fig. 1) continues northeastwards under the ice from the Ivisaartoq area 20-40 km to the south.

2. Geological Background

2.1. Archaean tectonostratigraphic terranes

The Archaean geology of southern West Greenland consists of tectonostratigraphic terranes (*sensu* Coney et al., 1980) of amphibolite-granulite facies gneisses. Detailed whole rock geochemical, isotopic and U-Pb zircon geochronological studies indicates

that they formed in environments with some similarities to Phanerozoic arcs (particularly intra-oceanic ones; e.g., McGregor et al., 1991; Polat and Hofmann, 2003; Polat et al., 2007; Dilek and Polat, 2008; Nagel et al., 2012; Nutman et al., 2013a). Through the Archaean, the arc-like complexes were progressively assembled into their present configurations by convergence and collisional orogeny, followed by intra-crustal reworking with granite production and shearing, to form more extensive areas of 'continental' crust (e.g., Friend et al., 1988; Nutman et al., 1989, 2010; 2013b; Nutman and Friend, 2007). Due the complexity of the geology, its vast area and overall similar lithologies, there must be reliance on U-Pb zircon geochronology to delimit individual terranes and understand their evolution. Thus knowledge of the disposition of the terranes and the implications for Archaean tectonic evolution has been evolving for 30 years, since Friend and Nutman first recognised terranes in the Færingehavn area (Friend et al., 1987; Friend and Nutman, 2005a; Nutman et al., this volume). Regardless of the incomplete understanding of details of terrane disposition, there is now broad consensus that the Archaean gneiss complex in Greenland (and similar ones elsewhere) are partitioned and evolved in this fashion, albeit there can be difference in the position and age of individual boundaries (e.g., Crowley, 2002; Hanmer and Greene, 2005; Windley and Garde, 2009).

In the study area the edge of the ice sheet overlaps the Isukasia terrane, which consists of Eoarchaean rocks (Fig. 1; Allaart et al., 1977; Nutman et al., 1996). The Eoarchaean geological record of the Itsaq Gneiss Complex is the most comprehensive in the world (Nutman et al., 1996; 2013a,b) and acts as a benchmark to compare the evolution of other Eoarchaean crustal fragments (Nutman, 2006). The Itsaq Gneiss Complex occurs as tectonic slices (tectonostratigraphic terranes) within a Neoarchaean orogen (Friend et al., 1988; Nutman et al., 1989; McGregor et al., 1991; Friend and Nutman, 2005). Most of the Itsaq Gneiss Complex was affected by 3660-3600 Ma high-grade metamorphism and ductile deformation causing widespread transformation of its igneous and sedimentary protoliths into multi-component amphibolite-granulite facies gneisses (Nutman et al., 1996, 2000, 2013b; Horie et al., 2010). The Itsaq Gneiss Complex is 95% strongly deformed

quartzo-feldspathic banded gneisses with rare areas of lesser deformation showing that these rocks were derived from plutonic tonalite and younger crustally-derived granite (*sensu stricto*) protoliths (Nutman et al., 2000; Horie et al., 2010).

To the south in the Ivisaartoq area there are Mesoarchaean (~3000 Ma) rocks belonging to the Kapisilik terrane (Fig. 1; Friend and Nutman, 2005a). Immediately north of Isua, reconnaissance SHRIMP U-Pb zircon dating of sample G07/44 (locality Fig. 1) indicates the presence of Mesoarchaean orthogneisses (Nutman, unpublished data), which we equate with the Kapisilik terrane. Farther to the north and west lies the Akia terrane, also consisting of Mesoarchaean gneisses (Friend et al., 1988; McGregor et al., 1991; Garde et al., 2001). At the edge of the ice sheet southeast of Nuuk, the Tasiusarsuaq terrane (Friend et al., 1987, 1988) is dominant, in which ~2950 – 2810 Ma orthogneisses affected by ~2800 Ma granulite facies metamorphism are most important (Fig. 1; Kinny, 1987; Schiøtte et al., 1989; Crowley, 2002; Næraa and Scherstén, 2008). The most northerly-recorded part of the Tasiusarsuaq terrane is on Nunataarsuk at ~64° 23'N (Fig. 1; Næraa and Scherstén, 2008).

Geology of the northern part of the craton along the edge of the ice front is only known from reconnaissance mapping (Allaart et al., 1978). By SHRIMP U-Pb zircon dating, Eoarchaean rocks with a strong Neoarchaean tectonothermal overprint have been reported from Aasivik at ~66°20'N (off the north of Fig. 1; Rosing et al., 2001;) and Qarliit tasersuat at ~65°46'N (Fig. 1; Nutman et al., 2004). Rosing et al. (2004) also reported Mesoarchaean gneisses just south of Aasivik at ~66°14'N. In the Discussion section of this paper, zircon results from the bedrock geology for the whole of the northern end of the Archaean craton (~63°30 to 70°N) are integrated with the glacial sand detrital zircon results presented here.

2.1. The Itsaq Gneiss Complex in the Isua – Ivisaartoq region

In and around the Isua supracrustal belt (ISB on Fig. 1) are most of the world's occurrences of Eoarchaean rocks that escaped upper amphibolite to granulite facies metamorphism (Allaart, 1976; Griffin et al., 1980; Nutman et al., 1996). In rare areas of low strain plutonic rocks preserve igneous textures and supracrustal rocks preserve

sedimentary and volcanic structures (e.g., Nutman and Bridgwater, 1986; Nutman et al., 1984; Komiya et al., 1989). A SHRIMP U-Pb zircon-dating programme with typical precision of ±5 Ma for rock ages demonstrated that the Isua supracrustal belt contains supracrustal rocks varying in age by ~100 million years, with the southern part of the belt dominated by ~3800 Ma rocks, whereas rocks of the northern and central portions are ~3700 Ma (Fig. 1; Nutman et al., 1996, 1997; 2013a, Crowley 2003; Kamber et al., 2005). These sequences with disparate ages are unrelated and are separated by Eoarchaean mylonites (Nutman et al., 1997, 2002, 2013a; Nutman and Friend, 2009). Despite some adherence to a concept that the Isua supracrustal belt comprises rocks of the same age (e.g., Moorbath, 2005), most recent workers have now adopted the interpretation that Isua contains supracrustal rocks of different age (e.g., Crowley, 2003; Rizo et al., 2011).

The Isua supracrustal belt is bounded to the north by ~3700 Ma orthogneisses cut by voluminous 3660-3630 Ma granite and pegmatite sheets (Nutman and Bridgwater 1986; Nutman et al., 1996, 2000, 2002; Crowley et al., 2002). Although superficially similar in appearance, on the south side of the Isua supracrustal belt are meta-tonalites older than those to the north, with ages of ~3800 Ma (Nutman et al., 1996, 1999, 2000; Crowley 2003). There are scattered indications that south of Isua older rocks are present. Thus on the northern part of Ivisaartoq there are ~3850 Ma orthogneisses (Nutman et al., 2007) and a granite ~5 km south of Isua carries ~3850 Ma xenocrystic zircon (Nutman and Friend, 2005b).

Volumetrically minor phases cutting the Itsaq Gneiss Complex are the meta-noritic and doleritic Ameralik dykes, most of which have ages of ~3500 Ma (Nutman et al., 2004). Additionally there are rare Neoarchaean pegmatites. In the Isua area the Itsaq Gneiss Complex was metamorphosed up to only epidote amphibolite facies conditions in the Neoarchaean (Nutman et al., 1996) and thus Neoarchaean metamorphic zircon is very rare. However, south towards the boundary with the Mesoarchaean Kapisilik terrane of Ivisaartoq, the Itsaq Gneiss Complex experienced higher grade metamorphism at ~2950 Ma and ~2690 Ma, as shown by the growth of metamorphic zircon with those ages (Friend and Nutman, 2005). The youngest

documented rocks in the area are post-kinematic early Palaeoproterozoic mafic dykes with an age of 2214 ± 10 Ma (Nutman et al., 1995).

3. Zirconology

3.1. Zircon sample collection, preparation and imaging

Sands #1 & 2 were collected from the river issuing from the ice on the south side of the Isua supracrustal belt, sand #3 was collected from a melt water river that flows westwards across the eastern end of the Isua supracrustal belt and sand #4 was collected ~20 km to the south on the eastern edge of the Ujaragssuit nunaat plateau (Fig. 1).

The sand samples were washed to remove organic matter and the mud-sized fraction and then dried. Zircon concentrates were prepared by heavy liquid and isodynamic separation techniques at the mineral separation laboratory of the Korean Basic Science Institute (KBSI). The non-magnetic fraction concentrates were hand-picked under a binocular microscope, and the selected grains were cast in epoxy resin discs together with the zircon Temora reference material (Black et al. 2003). The discs were ground to reveal mid-sections through the grains and then polished. The grains were documented with reflected and transmitted light photomicrographs and by cathodoluminescence (CL) imaging. CL images of representative zircons are shown in Fig. 2.

3.2. SHRIMP U-Th-Pb analytical method and data appraisal

Zircon U-Th-Pb isotopic analyses (Table 1) were undertaken with the SHRIMP II instrument at KBSI. Analytical protocols followed Williams (1998), and reduction of the raw data was undertaken using the software 'SQUID' (Ludwig, 2001). $^{206}Pb/^{238}U$ of the unknowns was calibrated using measurements of the Temora reference material (U-Pb ages concordant at 417 Ma; Black et al. 2003) interleaved with analyses of the unknowns. U and Th abundance was calibrated using measurement of the reference zircon SL13 (U=238 p.p.m.) located in a set-up mount. Common Pb corrections were undertaken using measured ^{204}Pb and the Cumming and Richards (1975) lead composition for the likely age of the grain. In all cases the amount of common Pb was assessed to be small (f^{206}% mostly <1%; Table 1).

The reduced and calibrated data were assessed and plotted using the ISOPLOT program of Ludwig (2003).

3.3. LA-MC-ICPMS analytical method

Zircon hafnium isotopic compositions were determined over a single analytical session using the RSES ThermoFinnigan Neptune multi-collector ICPMS coupled to a ArF λ=193 nm eximer 'HelEx' laser ablation system following methods described by Hiess et al. (2009). Owing to the small size of some of the zircons, the laser was focused to a 37 μm diameter circular spot firing at 5 Hz with an energy density at the sample surface of ~10 J/cm2. ^{171}Yb, ^{173}Yb, ^{174}Hf, ^{175}Lu, ^{176}Hf, ^{177}Hf, ^{178}Hf, ^{179}Hf and ^{181}Ta isotopes were simultaneously measured in static-collection mode on 9 Faraday cups with 10^{11} Ω resistors. A large zircon crystal from the Monastery kimberlite was used to tune the mass spectrometer to optimum sensitivity. Analysis of a gas blank and a suite of secondary reference zircons (Mud Tank, 91500, Temora-2 and FC1) were performed systematically after every 10-12 sample spot analyses.

Data was acquired in 1 s integrations over 100 s or until the grain ablated through. The segmental processing of the laser ablation data means that any down-hole variation in Lu/Hf and ^{176}Hf/^{177}Hf related to drilling through different growth zones can be detected. During data reduction on a custom Excel™ spreadsheet, time slices were cropped to periods maintaining steady ^{176}Hf/^{177}Hf signals. In the analyses presented in Table 2, Lu/Hf and ^{176}Hf/^{177}Hf ratios were uniform throughout data acquisition. Data reduction incorporated a within run dynamic amplifier correction. Total Hf signal intensity typically fell from >12 to 6 volts during a single analysis.

The measured ^{178}Hf/^{177}Hf, ^{176}Lu/^{177}Hf and ^{176}Hf/^{177}Hf ratios with 2σ uncertainties for the sample analyses are presented in Table 2 and the data for reference zircons is given in the Appendix Table A1. No corrections were required to normalize the measured ^{176}Hf/^{177}Hf ratios of standards to literature solution values.

Mass bias was corrected using an exponential law (Russell et al. 1978; Chu et al. 2002; Woodhead et al. 2004) and a composition for $^{179}Hf/^{177}Hf$ of 0.732500 (Patchett et al. 1981). As a quality check of this procedure, $^{178}Hf/^{177}Hf$ ratios for all zircon reference materials and samples are reported. Mean values of 1.46739 ± 9 (1 σ) and 1.46735 ± 3 lie within uncertainty of the value of 1.46735 published by Thirlwall and Anczkiewicz (2004). Yb and Lu mass bias factors were assumed to be identical and normalized using an exponential correction to a $^{173}Yb/^{171}Yb$ ratio of 1.129197 (Vervoort et al. 2004). The intensity of the ^{176}Hf peak was determined accurately by removing isobaric interferences from ^{176}Lu and ^{176}Yb. Interference-free ^{175}Lu and ^{173}Yb were measured and the interference peaks subtracted according to reported $^{176}Lu/^{175}Lu$ and $^{176}Yb/^{173}Yb$ isotopic abundances of Vervoort et al. (2004). Zircon $^{176}Lu/^{177}Hf$ ratios need to be accurately determined by LA-MC-ICPMS, to enable corrections for in-growth of radiogenic ^{176}Hf. Average measured $^{176}Lu/^{177}Hf$ ratios within the reference zircons (Mud Tank, 0.000012; 91500, 0.000328; Temora-2, 0.001123; FC1, 0.000934) are in good agreement with the solution values reported by Woodhead and Hergt (2005) of 0.000009, 0.000311, 0.001090 and 0.001262 respectively.

The mean $^{176}Hf/^{177}Hf$ ratios for each of the 4 reference zircons (Mud Tank: 0.282508±14; 91500: 0.282306±12; Temora-2: 0.282686±12; FC1: 0.282187±38 , 2σ) deviate from published solution values of Woodhead and Hergt (2005) by only +0.05, -0.01, +0.01 and +0.12 εHf units respectively (Appendix Table A1)). No correlation exists between $^{176}Hf/^{177}Hf$ and $^{178}Hf/^{177}Hf$, $^{174}Hf/^{177}Hf$ or $^{176}Lu/^{177}Hf$ ratios for any zircon reference materials, including the high Lu/Hf zircons, Temora-2 and FC1. This indicates that calculations for mass bias and Yb interference corrections were applied accurately. For the unknown zircons, initial $^{176}Hf/^{177}Hf$ ratios for each spot were calculated using their individual SHRIMP measured U-Pb ages, present day CHUR compositions of $^{176}Hf/^{177}Hf = 0.282785±11$, $^{176}Lu/^{177}Hf = 0.0336±1$ (Bouvier et al. 2008), and a $\lambda^{176}Lu$ decay constant of $1.867±8 \times 10^{-11} y^{-1}$ (Scherer et al. 2001; Söderlund et al. 2004).

Several sources of uncorrelated error may exist within these LA-MC-ICPMS

analyses that do not account for the external scatter seen in some reference zircons (e.g. 91500, Temora-2 and FC1). Therefore, a conservative approach is taken to estimate the absolute uncertainty of each spot that is used to calculate weighted mean εHf compositions. Within-run errors determined for individual analyses are summed in quadrature with an estimate of external reproducibility from the zircon reference materials, which was determined to be ±0.42 εHf units.

3.4. U-Th-Pb zircon results and grain morphology

Images of representative zircons are shown in Fig. 2. The populations are dominated by zircons with oscillatory zoning typical of grains of igneous origin. Some zircons show recrystallisation domains and some have overgrowths, typical of grains that have experienced high grade metamorphism. The interior zonation is largely parallel to the grain exteriors, indicating only limited abrasion during surface transport.

All 305 zircon U-Pb analyses are presented on a Tera-Waserburg Concordia diagram (Fig. 3). Approximately 80% of the analyses have near concordant ages, and all are Archaean, with one early Palaeoproterozoic exception. Prior to constructing cumulate frequency distribution and histogram diagrams (Fig. 4) data with >10% difference in $^{238}U/^{206}Pb$ and $^{207}Pb/^{206}Pb$ age (~20% of the analyses) were rejected. There is significant variation in degree of grain rounding with age. This suggests that transport distances for all grains is similar. Data from the three Isua sands were pooled, whereas the sand from eastern Ujaragssuit nunaat was assessed separately.

In the 3 Isua sands (samples #1 to 3) Neoarchaean grains are more abundant than Eoarchaean ones (Fig. 4a). Two main subpopulations of Neoarchaean grains are evident, one with ~2830, 2805 and 2790 Ma sub-peaks and the other with ~2730, 2710 and 2695 Ma sub-peaks. A few grains show younger Neoarchaean ages. None of these zircon ages have been encountered in the bedrocks at Isua, apart from one rare ~2695 Ma metamorphic overgrowth (Nutman et al., 1997). One early Palaeoproterozoic grain (grain 36 in sand #3 with a $^{207}Pb/^{206}Pb$ age of 2414 Ma) was detected. In the Eoarchaean grains several populations are evident. Those from ~3800

to 3600 Ma match the age of the two terranes and granite production following their ~3660 Ma juxtaposition (Nutman et al., 2013b and references therein). Two other populations are present at a small percentage, at ~3850 and 3890 Ma (Fig. 4a). From the bedrocks of the Isua area ≥3840 Ma ages are only known as very rare detrital components in >3700 Ma sedimentary rocks of the Isua supracrustal belt (Nutman et al., 1997; 2009). Finally, a single >3900 Ma grain was detected (grain 51, sand #1). Duplicate analyses on this grain gave $^{207}Pb/^{206}Pb$ ages of 3958 ± 10 and 3976 ± 16 Ma (2σ; Table 1). This grain has a similar age to the oldest detrital grain (3942 ± 51 Ma) found in Isua supracrustal belt rocks (Grain 4 of sample G07/22 in Nutman et al., 2009).

In the single sand sample (#4) from eastern Ujaragssuit nunaat, there is again a broad division into Neo- and Eoarchaean sub-populations, but with a different bias (Fig. 4b). In the eastern Ujaragssuit nunaat sand, 2840 and 2805 Ma grains are important, with only a few younger Neoarchaean grains detected. Additionally there is a peak at ~2960 Ma, which corresponds to the timing of a metamorphic event on Ujaragssuit nunaat, recorded by low Th/U zircon overgrowths (Nutman et al., 2002; Friend and Nutman, 2005; Nutman et al., this volume). In the Eoarchaean subpopulation 3800-3600 Ma grains are important, but the single largest grouping is at ~3850 Ma (Fig. 3b). ~3850 Ma orthogneisses have been documented on northern Ivisaartoq, ~20 km to the south (Fig. 1b; Nutman et al., 2007). The results from sand #4 shows that rocks of this age are also found under the ice cap.

Combining the Isua and Ujaragssuit nunaat sand data onto a single Th/U versus $^{207}Pb/^{206}Pb$ age plot shows that in both the Eoarchaean and Neoarchaean subpopulations the data form approximately triangular fields, such that the oldest grains in each group show Th/U of typically ~ 1 to 0.3, whereas in the youngest ones the range has widened to ~1 to ~0.01 (Fig. 5a). This will be commented on in the Discussion, as will be the general lack of Mesoarchaean grains in the sands.

3.5. Hf isotopic results

Grain CL imagery and SHRIMP U/Pb geochronological results were used to

select sites with concordant ages and least evidence of recrystallisation for Hf isotopic analysis. Ninety-three analyses were performed on zircons from the Isua sands and 36 from the eastern Ujaragssuit nunaat sand (Table 2). Most of the laser ablation Hf analysis sites were located directly over the shallow (<2μm) SHRIMP analysis pits. Monitoring of any down-hole variation in Lu/Hf and $^{176}Hf/^{177}Hf$ was used to ensure that the final result did not represent compositional mixtures. The data are presented as a $\varepsilon Hf_{(t\text{-}zirc)}$ versus $^{207}Pb/^{206}Pb$ age (≈ t-zirc) plot (Fig. 5b).

Throughout the age range from ~3900 to 3640 Ma there are grains with $\varepsilon Hf_{(t\text{-}zirc)}$ values of ~0 (CHUR-like; Fig. 5b), demonstrating repeated additions of juvenile material to the crust throughout this interval (e.g., Hiess et al., 2009; Bennett et al., 2007). Hf model ages for >3.7 Ga grains (Table 2) span a narrow range from 3720 to 3920 Ma providing no evidence for reworking of Hadean crustal materials. Regrettably, the oldest grain detected (grain 51, sand sample #1) was too thin on the mount to produce reliable Hf isotopic data. At ⩽3800 Ma and particularly at 3650-3600 Ma there are also grains with sub-CHUR values to ~ -3, with 2-stage model ages largely between 3700 and 3900 Ma (Table 2). The most likely explanation is that these grains are products of crustal recycling of slightly older (≤3900 Ma juvenile crust), as is recorded in the isotopic signatures of granitic rocks of that age in the Isukasia terrane (Baadsgaard et al., 1986; Hiess et al., 2010). However, it cannot be discounted that some of these sub-CHUR values result from underestimate of the crystallization age due to minor ancient Pb loss.

In the Neoarchaean sub-population, grains with ~2950 to 2840 Ma ages have super-chondritic $\varepsilon Hf_{(t\text{-}zirc)}$ of ~ +2 to +5, demonstrating extraction of juvenile crust from a mantle previously depleted in Hf versus Lu (Fig. 5b). Grains from ~2840 to ~2790 Ma show declining $\varepsilon Hf_{(t\text{-}zirc)}$ values, to ~ -3. This can be accommodated by tectonothermal recycling of the ~2960 to 2840 Ma crustal components. <2720 Ma Neoarchaean grains show a much greater spread of $\varepsilon Hf_{(t\text{-}zirc)}$ values, down to ~ -24 with a commensurate large range of Hf model ages. This variation is best accommodated by variable amounts of recycling of Eoarchaean crust. Analyses such as grain 20 in Isua sand #2 and also grain 20 in sand #3 are of low Th/U <2720 Ma

homogeneous rims over oscillatory zoned cores (Fig. 2). Grain 47 in sand #2 is an example of an entirely recrystallised prismatic grain, with low Th/U and $\varepsilon Hf_{(t\text{-}zirc)}$. These relationships suggest *in situ* metamorphic recrystallisation of Eoarchaean zircons, rather than being new igneous zircons produced by the remelting of Eoarchaean rocks.

4. Discussion

4.1. Age signature of detrital zircons and known tectonostratigraphic terranes

Zircon U-Pb ages for magmatic and tectonothermal events in the terranes of the Nuuk region are plotted in Figure 4C to compare with the age spectra of the sand sample zircons. The Itsaq Gneiss Complex is dominated by pulses of tonalitic-dioritic crustal additions from ~3890 Ma to 3660 Ma (Nutman et al., 1996, 2000, 2007; Crowley et al., 2002; Crowley, 2002; Hiess et al., 2009; Horie et al., 2010). This was followed by the Isukasian orogeny involving high temperature metamorphism in the lower crust, with production of 3650-3600 Ma crustally-derived granites (Baadsgaard et al., 1986; Nutman et al., 1996, 2013b). The results from the sands mimic the ages of the bedrock of Itsaq Gneiss Complex, but it is worth noting the appreciable amount of >3820 Ma zircons in the sand samples. These show peaks at ~3850 and 3890 Ma, which matches known ages of small parts of the exposed Itsaq Gneiss Complex (Nutman et al., 2007; Hiess et al., 2009; Horie et al., 2010). However the strong representation of these zircons in the sand samples indicates that 'pre-Isua' >3820 Ma crust is important under the ice cap between northern Ivisaartoq and Isua, where they are only known from an inherited zircon in a granite (Friend and Nutman, 2005b) and as rare detrital grains in ≥3700 Ma Isua supracrustal belt sedimentary rocks (Nutman et al., 1997, 2009). Despite 305 zircon analyses, no Hadean (>4000 Ma) grains were detected. Thus even if a Hadean component formed only 1% of the source region, then there would be a <0.05 probability of missing it after 305 analyses (using the relationship $P=(1-x)^n$; where P=probability, x=proportion of non-detected component and n=grains analysed). In keeping with knowledge of the exposed parts of the Itsaq Gneiss Complex, this indicates it is extremely unlikely that Hadean crust is hidden

under the icecap.

A key feature that is evident from both the Isua and the eastern Ujaragssuit nunaat sands is the paucity of early Mesoarchaean zircons that would match the Kapisilik terrane rock ages (Figs. 3 and 4), whereas along the ice edge to both the south and north of the sand sampling sites the bedrocks are dominated by the 3250-2970 Ma Kapisilik and Akia terranes (Figs. 1 and 4; Garde et al., 2001; Friend and Nutman, 2005; Garde, 2007; Næraa et al., 2012; Nutman et al., this volume). Clearly the Kapisilik and Akia terranes are not present under the ice east of the sand sampling sites. The few detected early Mesoarchaean grains have low Th/U ratios (Fig. 5A), suggesting that they reflect recrystallisation or metamorphic events, rather than the rock-forming events seen in the Kapisilik and Akia terranes.

The late Mesoarchaean to early Neoarchaean components (~2950 to 2790 Ma) matches rocks that are found within the Tasiusarsuaq and Tre Brødre terranes (Kinny, 1987; Schiøtte et al., 1989; Crowley, Friend and Nutman, 2001; Nutman and Friend, 2007; Friend et al., 2009; Næraa et al., 2012; Fig. 4C). Plutonic rocks of the Tre Brødre terrane have an essentially unimodal age at ~2825 Ma with ~2840 Ma volcano-sedimentary rocks also present (Nutman et al., 2004; Nutman and Friend, 2007; Fig. 4C). The Neoarchaean age components of the Tasiusarsuaq terrane are much more complex, with 2950-2920, 2870-2840 Ma and 2810-2800 Ma rocks present, with superimposed 2800-2790 Ma granulite facies metamorphism in its northern parts (Fig. 4C). Additionally, the northern edge of the Tasiusarsuaq terrane in Ameralla (Fig. 1) locally contains migmatites with Eoarchaean and 2860-2800 Ma components (samples 437605 and G03/18; Figs. 1 and 4c; Table 1). Thus it is likely that the 2950-2790 Ma zircons were sourced from a northern extension of the Tasiusarsuaq terrane. This is in keeping with the presence of exotic blocks of granulite facies rocks in moraines in the Isua area. These granulites cannot be locally-sourced, because the Itsaq Gneiss Complex of Isua and eastern Ujaragssuit nunaat only experienced amphibolite facies metamorphism (Griffin et al., 1980; Nutman et al., 1996), whereas granulite facies metamorphism is common in the northern end of the Tasiusarsuaq terrane (Wells, 1976; Friend et al., 1988; Nutman et al., 1989; Crowley,

2002).

4.2. Hf isotopic signature and crustal evolution

The integrated sand detrital zircon U-Pb dating and Hf isotopic results indicate two main episodes of juvenile crust formation in the source region, one at 3880 to ≤3700 Ma with $\varepsilon Hf_{(t\text{-}zirc)} \approx 0$ and again in the Neoarchaean from 2950 to 2840 Ma with mildly positive $\varepsilon Hf_{(t\text{-}zirc)}$. The supra-CHUR $\varepsilon Hf_{(t\text{-}zirc)}$ values for the 2950 to 2840 Ma zircons are particularly significant, because they demonstrate no involvement of significantly older crust, even though Eoarchaean rocks are clearly present in the same sand source region. Within each of these events there is granularity, thus in the Eoarchaean episode there is a hiatus between crust formation finishing at ~3800 Ma, and crust formation starting again at ~3720 Ma (Figs. 4 and 5B). This suggests that the two source regions evolved separately until after ~2800 Ma. However from ~2720 Ma onwards zircons (commonly low Th/U metamorphic overgrowths or entirely recrystallised grains; Fig. 2) show a broad range of $\varepsilon Hf_{(t\text{-}zirc)}$ from ~ -2.5 to -24, indicating both the Neo- and Eoarchaean crustal segments experienced a common tectonothermal event (Fig. 5B). This is in accord integrated structural, metamorphic and zircon dating studies of the bedrocks in the Nuuk region, which demonstrates ~2700 Ma juxtaposition with crustal thickening of the Itsaq Gneiss Complex (Færingehavn and Isukasia terranes) with the Tre Brødre and Tasiusarsuaq terranes (Nutman et al., 1989, Friend et al., 1996; Crowley, 2002; Nutman and Friend, 2007).

4.3. Zircon provenance and terrane mapping under the ice

Meirebachtol et al., (2013) examined basal drainage system response to increasing surface melt on the Greenland ice sheet, by monitoring water pressure in seven boreholes in the ice of the glacier Isunnguata Sermia (central West Greenland). They noted that boreholes nearer to the edge of the ice experience big fluctuations in pressure, pointing to connectivity and rapid response to the variable influx of surface waters down cracks. On the other hand, boreholes distal from the ice edge showed little fluctuation which was interpreted to show a hydrological regime of linked

cavities were restricted connectivity maintained high constant pressure, low water velocities and hence little potential for erosion. On the other hand, proximal to the ice front basal water flow is highly channelised, with periods of high velocity promoting erosion of the bedrock and transport of debris. Based on borehole measurements, and mathematical modeling the Meierbachtol et al. (2013) results signify that the sediment issuing from under Isunnguata Sermia is sourced from less than 100 km away, and most likely within 30 km. Although there will be some differences in physical conditions between Isunnguata Sermia and the Isua area, the principle will be the same – sediment will be sourced from under the fringe of the ice cap.

The evidence that basal erosion is most prevalent near the ice fringe is in keeping with ~50% of the zircons being sourced from Eoarchaean rocks – like those that are exposed along the ice front. The results of Meirebachtol et al. indicate that the Neoarchaean zircons (with an age and Hf isotopic signature like the Tasiusarsuaq and Tuno terranes; Fig. 4c) most likely come from much less than 100 km east of the ice front. Such a model is compatible with regional structural trends, as is portrayed in Figure 1. In contrast, the sands appear to be devoid of detritus from the Mesoarchean Kapisilik terrane, which is exposed at the margin of the ice cap from ~40 km south of Isua in the Ivisaartoq region and also north of Isua (Figure 1). We suggest that the Kapisilik terrane was truncated by a Neoarchaean tectonic boundary, which led to the juxtaposition of the Itsaq Gneiss Complex and the Tasiusarsuaq terranes under the ice cap, east of Isua (Fig. 1).

Based on the likelihood that the melt-water sands were sourced from close to the edge of the ice cap, the detrital zircon age spectra can be integrated with aeromagnetic coverage that extends into the fringe of the ice cap (Rasmussen and Thorning, 1999) and the geology exposed near the ice front. The Tasiusarsuaq terrane is prevalent along the ice front in the southern part of the Nuuk region (Fig. 1). Structural syntheses have generally regarded that the boundary of the Tasiusarsuaq terrane heads eastwards under the ice (Friend et al., 1987 and onwards). However, the eastern part of Nunataarsuk (a nunatak east of Nuuk; Fig. 1) consists of anorthosites and amphibolites intruded by 2852 ± 5 Ma orthogneisses (Næraa and Scherstén, 2008).

This age matches that of major components in the Tasiusarsuaq ± Tre Brødre terranes, but *not* the Kapisilik terrane (Fig. 4c). A major north-south trending metamylonite separates these rocks from ones that are structurally contiguous with the Kapisilik terrane to the west (Fig. 1). Under the edge of the ice to the east of the Nuuk region is a prominent gradient in the aeromagnetic signature, which appears to truncate the blotchy, more magnetised signature of the Kapisilik terrane and also traverses eastern Nunataarsuk (Fig. 1). We contend that the original ~3000 Ma tectonic boundary between the Itsaq gneiss complex Isukasia terrane and the Kapisilik terrane on southern Ujaragssuit nunaat (Friend and Nutman, 2005a) is truncated under the ice by a younger Archaean tectonic boundary, such that the Kapisilik terrane has been excised and in the north the Tasiusarsuaq ± Tre Brødre and Isukasia terranes are in contact (Fig. 1). In the southern part of the Nuuk region, zircon U-Pb dating constrains the juxtaposition of the Tasiusarsuaq with other terranes in the Neoarchaean at ~2700 Ma (Friend et al., 1996; Crowley, 2002; Nutman and Friend, 2007). We suggest that the boundary of the Tasiusarsuaq terrane under the ice in the Isua area is also of this age, because the zircon U-Pb-Th-Hf data show the recrystallisation of Eoarchaean zircons in a tectonothermal event at that time (Fig. 5). The massive positive aeromagnetic anomaly of the magnetite-rich iron ore deposit at Isua is truncated ~5 km east of the ice front (Fig. 1). Thus, as a point of economic geology interest, it is possible that the proposed Neoarchaean tectonic boundary is responsible for the truncation of the Isua iron ore deposit. This interpretation requires that the boundary of the Tasiusarsuaq terrane swings north-northwestwards, such that it is nearer the ice front in the Isua area than off eastern Ujaragssuit nunaat. This would be in accord with the Isua sands containing a slightly larger proportion of Neoarchaean zircons than found in the Ujaragssuit nunaat sand (57% versus 49% respectively) and also a swing north-northwestwards in the aeromagnetic gradient that is interpreted as the terrane boundary (Fig. 1).

4.4. Simple or complex Archaean terrane boundaries in West Greenland?

Since the recognition that the west Greenland Archaean gneiss complex is a

mosaic of unrelated crustal blocks that were juxtaposed later in the Archaean by collisional orogeny (Friend et al., 1987) there have been several attempts to produce an Archaean tectonic synthesis for the whole region (e.g., McGregor et al., 1991; Windley and Garde, 2009). Most of these have recognised that the tectonic terrane boundaries were folded, deformed and metamorphosed in later Archaean events (shown in red in Fig. 1 of this paper and as was explicitly shown in Figs. 1 and 2 of Friend et al., 1987 – the first paper on this subject). This exacerbates the extrapolation of terrane boundaries into areas with lesser amounts of detailed mapping and reliable zircon U-Pb geochronological data. Also present are essentially straight Neoarchaean tectonic boundaries such as the Ivinguit fault separating the Akia terrane from several terranes to the east (Fig. 1; McGregor et al., 1991). Most syntheses have interpreted these as a later structures (~2530 Ma) cross-cutting the original (>2650 Ma) terrane assembly boundaries (e.g., Friend and Nutman, 2005; Nutman et al., 2010).

North of Isua, rocks with ages matching those of the Tasiusarsuaq terrane are not encountered until the Tuno terrane (Fig. 4C) in the far north of the Craton, off the northern edge of Figure 1 (Friend and Nutman, 1994; Nutman and McGregor, unpublished data). This suggests possible linkages between rocks that were previously thought to be unrelated in all syntheses. In this interpretation, the northern edge of Tasiusarsuaq terrane disappears under the ice cap east of Godthåbsfjord. However it then swings north, such that its components appear within the sand samples studied in this paper. It next emerges from under the ice cap in a fold core as the Qarliit tasersuat assemblage (Nutman et al., 2004), a group of rocks with Eoarchaean components overprinted by early Neoarchaean tectonothermal events (2781 ± 8 Ma and 2767 ± 5 Ma). Such events are seen in the northern Tasiusarsuaq (e.g. sample 437605; 2767 ± 5 Ma; Fig. 4C) and the Tuno terrane farther north. Mesoarchaean gneisses like those of the Akia terrane reappear at the ice front north of the Qarliit tasersuat (sample VM97/19 on Fig. 1; Nutman and McGregor, unpublished data). Therefore northwards, the extension of the Tasiusarsuaq terrane is again obscured under the ice cap. We contend that it links in the far north of the craton with the Tuno terrane, which together with the Qarliit tasersuat assemblage contains similar age components to the

northern parts of the Tasiusarsuaq terrane and the Isua area glacial sands.

In a radical departure to this view, Windley and Garde (2009) proposed a much simpler synthesis, with division of the Archaean gneiss complex north of 62°N into tilted crustal sections forming linear, tabular terranes running approximately SW-NE to E-W (shown in Fig. 1 with blue lines). As pointed out by Nutman et al. (2010), some of the boundaries proposed by Windley and Garde cut orthogonally across both fold structures mapped in detail and aeromagnetic gradients, and ignore the ages of the rocks.

In previous tectonic models, the Tasiusarsuaq terrane has been interpreted as having developed in the late Meso- to early Neoarchaean as a complex arc-like assemblage, which in the Neoarchaean collided with other terranes, such as the Færingehavn terrane (Friend et al., 1987, 1988; McGregor et al., 1991). The likelihood that the Tasiusarsuaq terrane continues northwards under the ice cap and truncates the boundary between the Isuakasia and Kapisilik terranes is further evidence of the complexity of Archaean terrane boundary evolution, and is evidence contrary to the simplified interpretation presented by Windley and Garde.

Between Isua and Qarliit tasersuat the edge of the Akia terrane is fringed by a thick package of metasedimentary rocks, which extend out to a large nunatak (Fig. 1). These rocks were mapped at a reconnaissance scale for compilation of a 1:500,000 geological map (Allaart et al., 1978; Allaart, 1982), but have not been investigated since the 1970s. However we note that on the coast to the west, north of Maniitsoq at Hamborgerland (at 66°32’N 52°57’W off the eastern edge of Figure 1), the boundary between the Akia and Tuno terranes is marked by a thick package of amphibolite-granulite facies metasedimentary rocks, in which the detrital zircons were derived from sources matching >2800 Ma components of the Tuno and Tasiusarsuaq terranes, plus the Akia terrane (Nutman et al., 2004). The metasedimentary rocks along the ice front between Qarliit tasersuat and Isua could be a continuation of the package at Hamborgerland. If so, this would further strengthen a linkage between the Tuno and Tasiusarsuaq terranes. The proposal in this paper for a linkage/correlation between the Tasiusarsuaq and Tuno terranes shows that the collision between it and

other terrane(s) was not an event restricted to the Nuuk region, but is of craton-wide significance. This requires a reappraisal of Archaean crustal evolution and terrane assembly in West Greenland, particularly in the northern part of the craton (Nutman et al., in preparation).

5. CONCLUSIONS

(1) Zircons from melt water rivers near the Isua supracrustal belt and ~20 km to the south on eastern Ujaragssuit nunaat contain mostly Eoarchaean and Neoarchean zircons. >2950 Ma Mesoarchaean grains are largely absent and Hadean crust was not detected.

(2) The integrated U-Pb geochronology and Hf isotopic data show that the grains are sourced from two unrelated juvenile crust formation events (3880-3600 and 2950-2800 Ma). The zircon ages match the Itsaq Gneiss Complex Isukasia terrane and the Tasiusarsuaq terrane respectively. There is no evidence that the source region contains rocks of the early Mesoarchaean Akia and Kapisilik terranes.

(3) The Hf isotopic data shows that Eoarchaean crust did not participate in 2950-2800 Ma crust formation, whereas at ~2700 Ma both the late Meso- and Eoarchaean juvenile crustal zircons developed metamorphic overgrowths or were recrystallised. This demonstrates the juxtaposition of disparate terranes and a common tectonothermal history by ~2700 Ma.

(4) Aeromagnetic signatures suggests that a ~2700 Ma(?) western boundary of the Tasiusarsuaq terrane continues northwards under the ice, and truncates the ~3000 Ma tectonic boundary between the Isukasia and Kapisilik terranes. The boundary might swing northwestwards to within 5 km of the ice front in the Isua area, and truncate the eastern end of the iron ore deposit. This would explain why there are more Neoarchaean detrital zircons in the Isua sands than in the eastern Ujaragssuit one.

(5) The proposed truncation of the ~3000 Ma tectonic boundary between the Isukasia and the Kapisilik terranes by the western ~2700 Ma tectonic

boundary of the Tasiusarsuaq terrane points to complex, terrane assembly and reconfiguration in several unrelated events, as proposed in models such as Friend and Nutman (2005a). The data presented here does not support the simpler terrane synthesis presented by Windley and Garde (2009).

ACKNOWLEDGEMENTS

Current work on the Itsaq Gneiss Complex is supported by Australian Research Council Discovery Grant DP120100273 and the Korean Basic Science Institute. Ole Christiansen and Nunaminerals A/S are thanked for logistical support in Greenland

REFERENCES CITED

Allaart, J. H., 1976. The pre-3760 m.y. old supracrustal rocks of the Isua area, central West Greenland, and the associated occurrence of quartz-banded ironstone. In: Windley, B.F. (Ed), The Early History of the Earth. Wiley, London, pp. 177-189.

Allaart, J.H., 1982. 1:500,000 scale geological map sheet Frederikshåb Isblink – Sondre Strømfjord (63°30’ - 66°45’N). Geological Survey of Greenland and Denmark, Copenhagen

Allaart, J.H., Jensen, S.B., McGregor, V.R., Walton, B.J., 1977. Reconnaissance mapping for the 1:500 000 map sheet in the Godthåb-Isua region, southern West Greenland. Grønlands Geologiske Undersøgelse Rapport 85, 50-54.

Baadsgaard, H., Nutman, A. P., and Bridgwater, D., 1986. Geochronology and isotope geochemistry of the early Archaean Amîtsoq gneisses of the Isukasia area, southern West Greenland. Geochimica et Cosmochimica Acta 50, 2173-2183.

Black, L.P., Kamo, S.L., Allen, C.M., Aleinikoff, J.M., Davis, D.W., Korsch, R.J., Foudoulis, C., 2003. TEMORA 1: A new zircon standard for Phanerozoic U-Pb geochronology. Chemical Geology 200**,** 155-170.

Bouvier A., Vervoort J.D., Patchett J., 2008. The Lu–Hf and Sm–Nd isotopic composition of CHUR: constraints from unequilibrated chondrites and implications for the bulk composition of the terrestrial planets. Earth and Planetary Sciences Letters, 280, 285-295, doi:10.1016/j.epsl.2008.06.010.

Chu, M-F., Chun, S-L., Song, B., Liu, D-Y., O'Reilly, S.Y., Pearson, N.J., Ji, J., Wen, D-J., 2002. Zircon U-Pb and Hf isotope constraints on the Mesozoic tectonics and crustal evolution of southern Tibet. Geology 34, 745-748, doi: 10.1130/G22725.1.

Coney, P.J., Jones, D.L., Monger, J.W.H., 1980. Cordilleran suspect terranes. Nature 288, 329–333, doi: 10.1038/288329a0.

Crowley, J.L., 2002. Testing the model of late Archaean terrane accretion in southern West Greenland: a comparison of the timing of geological events across the Qarliit nunaat fault, Buksefjorden region. Precambrian Research 116, 57-80.

Crowley, J.L., 2003. U-Pb geochronology of 3810-3630 Ma granitoid rocks south of the Isua greenstone belt, southern West Greenland. Precambrian Research 126, 235-257.

Crowley, J.L., Myers, J.S., Dunning, G.R., 2002. The timing and nature of multiple 3700-3600 Ma tectonic events in granitoid rocks north of the Isua greenstone belt, southern West Greenland. Geological Society of America Bulletin 114 1311-1325.

Cumming, G.L., Richards, J.R. 1975, Ore lead ratios in a continuously changing Earth. Earth and Planetary Science Letters, 28, 155-171.

Dilek, Y., Polat, A., 2008. Suprasubduction zone ophiolites and Archean tectonics. Geology 36, 431–432, doi:10.1130/Focus052008.1.

Friend, C.R.L., Nutman, A.P., 1994. Two Archaean granulite-facies metamorphic events in the Nuuk-Maniitsoq region, southern West Greenland: correlation with the Saglek block, Labrador. Journal of the Geological Society of London 151, 421-424.

Friend, C.R.L., Nutman, A.P., 2001. U-Pb zircon study of tectonically bounded blocks of 2940-2840 Ma crust with different metamorphic histories, Paamiut region, South-West Greenland: implications for the tectonic assembly of the North Atlantic craton. Precambrian Research 115, 143-164.

Friend, C.R.L., Nutman, A.P., 2005a. New pieces to the Archaean terrane jigsaw puzzle in the Nuuk region, southern West Greenland: Steps in transforming a simple insight into a complex regional tectonothermal model. Journal of the Geological Society of London 162, 147-163.

Friend, C.R.L., Nutman, A.P., 2005b. Complex 3670–3500 Ma orogenic episodes superimposed on juvenile crust accreted between 3850–3690 Ma, Itsaq Gneiss Complex, southern West Greenland. Journal of Geology 113, 375-397.

Friend, C.R.L., Nutman, A.P., McGregor, V.R., 1987. Late Archaean tectonics in the Færingehavn - Tre Brødre area, Budsefjorden, southern West Greenland. Journal of the Geological Society, London 144, 369-376.

Friend, C.R.L., Nutman, A.P., McGregor, V.R., 1988. Late Archaean terrane accretion in the Godthåb region, southern West Greenland. Nature, 335, 535-538.

Friend, C.R.L., Nutman, A.P., Baadsgaard, H., McGregor, V.R., Kinny, P.D., 1996. Timing of late Archaean terrane assembly, granite emplacement and metamorphism in the Nuuk region, southern West Greenland. Earth and Planetary Science Letters 142, 353-366.

Friend, C.R.L., Nutman, A.P., Baadsgaard, H. & Duke, J., 2009. The whole rock Sm-Nd 'age' for the 2825 Ma Ikkattoq gneisses (Greenland) is 800 Ma too young: Insights into Archaean TTG petrogenesis. Chemical Geology, 261, 61-75.

Garde, A.A., 2007. A mid-Archaean island arc complex in the eastern Akia terrane, Godthåbsfjord, southern West Greenland. Journal of the Geological Society, London 164, 565-579.

Garde, A.A., Friend, C.R.L., Marker, M., Nutman, A.P., 2001. Rapid maturation and stabilisation of middle Archaean continental crust: the Akia terrane, southern West Greenland. Bulletin of the Geological Society of Denmark 47, 1-27.

Griffin, W.L., McGregor, V.R., Nutman, A.P., Taylor, P.N., Bridgwater, D., 1980. Early Archaean granulite-facies metamorphism south of Ameralik. Earth and Planetary Science Letters 50, 59-74.

Hiess, J., Bennett, V. C., Nutman, A. P., Williams, I. S., 2009. In situ U–Pb, O and Hf isotopic compositions of zircon and olivine from Eoarchaean rocks, West Greenland: New insights to making old crust. Geochimica et Cosmochimica Acta 73 4489–4516.

Hiess, J., Bennett, V.C., **Nutman, A.P.** & Williams, I.S.: Archaean fluid-assisted crustal cannibalism recorded by low $\delta^{18}O$ and negative $\varepsilon_{Hf(T)}$ isotopic signatures of West Greenland granite zircon. Contributions to Mineralogy and Petrology, DOI: 10.1007/s00410-010-0578-z.

Hoffmann, J.E., Münker, C., Næraa, T., ROSING, M.T., 2011. Mechanisms of Archean crust formation inferred from high-precision HFSE systematics in TTGs. Geochimica et Cosmochimica Acta 75, 4157-4178.

Horie, K., Nutman, A.P., Friend, C.R.L., Hidaka, H., 2010. The complex age of orthogneiss protoliths exemplified by the Eoarchaean Itsaq Gneiss Complex (Greenland): SHRIMP and old rocks. Precambrian Research 183, 25-43.

Kamber, B.S., Whitehouse, M.J., Bolhar, R., Moorbath, S. 2005. Volcanic resurfacing and the early terrestrial crust: Zircon U-Pb and REE constraints from the Isua Greenstone Belt, southern West Greenland. Earth and Planetary Science Letters **240**, 276-290.

Kemp, A.I.S., Foster, G.L., Scherstén, A., Whitehouse, M.J., Darling, J., Storey, C., 2009. Concurrent Pb-Hf isotope analysis of zircon by laser ablation multi-collector ICP-MS, with implications for the crustal evolution of Greenland and the Himalayas. Chemical Geology 261, p. 244-260.

Kinny P.D., 1987. Uranium-lead and hafnium isotopes in zircon. PhD thesis (unpublished), Australian National University.

Komiya, T., Maruyama, S., Masuda, T, Appel, P.W.U., Nohda, S., 1999. The 3.8-3.7 Ga plate tectonics on the Earth; Field evidence from the Isua accretionary complex, West Greenland. Journal of Geology 107, 515-554.

Ludwig, K.R., 2001. Squid 1.02: A User's Manual. Berkeley Geochronology Center Special Publication No.2, 1-19.

Ludwig, K.R., 2003. Isoplot/Ex. Berkeley Geochronology Center, Publication 1.

McGregor, V.R., 1973. The early Precambrian gneisses of the Godthåb district, West Greenland. Philosophical Transactions of the Royal Society of London A273, 343-358.

McGregor, V.R., Friend, C.R.L. & Nutman, A.P., 1991. The late Archaean mobile belt through Godthåbsfjord, southern West Greenland: a continent-continent collision zone? Bulletin of the Geological Society of Denmark 39, 179-197.

Meierbachtol, T., Harper, J., Humprey, N., 2013. Basal drainage system response to increasing surface melt on the Greenland ice sheet. Science, 341, 777, 779.

Moorbath, S., 2005. Oldest rocks, earliest life, heaviest impacts, and the Hadean–Archaean transition. Applied Geochemistry 20, 819–824.

Nagel, T.J., Hoffmann, J.E., Münker, K., 2012. Generation of Eoarchean tonalite-trondhjemite-granodiorite series from thickened mafic arc crust. Geology 40, 375-378; doi:10.1130/G32729.1

Nielsen, S.G., Baker, J.L., Krogstad, E.J., 2002. Petrogenesis of an early Archaean (3.4 Ga) norite dyke, Isua, West Greenland: evidence for early Archaean crustal recycling? Precambrian Research, 118, 133-148.

Nutman, A.P., 2001. On the scarcity of >3900 Ma detrital zircons in ≥3500 Ma metasediments. Precambrian Research, 105, 93-114.

Nutman, A.P., 2006. Antiquity of the oceans and continents. Elements 2, 223-227.

Nutman, A.P., Bridgwater, D., 1986, Early Archaean Amîtsoq tonalites and granites from the Isukasia area, southern West Greenland: Development of the oldest-known sial. Contributions to Mineralogy and Petrology 94, 137-148.

Nutman, A.P., Friend, C.R.L., 2007. Terranes with ca. 2715 and 2650 Ma high-pressure metamorphisms juxtaposed in the Nuuk region, southern West Greenland: Complexities of Neoarchaean collisional orogeny. Precambrian Research 155, 159-203.

Nutman, A.P., Friend, C.R.L., 2009. New 1:20000 geological maps, synthesis and history of the Isua supracrustal belt and adjacent gneisses, Nuuk region, southern West Greenland: A glimpse of Eoarchaean crust formation and orogeny. Precambrian Research 172, 189-211.

Nutman, A.P., Friend, C.R.L., Baadsgaard, H., McGregor, V.R., 1989. Evolution and assembly of Archaean gneiss terranes in the Godthåb region, southern West Greenland: Structural, metamorphic and isotopic evidence. Tectonics 8, 573-589.

Nutman, A.P., Friend, C.R.L., Bennett, V., 2004. Dating of the Ameralik dyke swarms of the Nuuk district, southern West Greenland: Mafic intrusion events starting from c. 3510 Ma. Journal of the Geological Society, London 161, 421-430.

Nutman, A.P., McGregor, V.R., Friend, C.R.L., Bennett, V.C., Kinny, P.D., 1996. The Itsaq Gneiss Complex of southern West Greenland; the world's most extensive record of early crustal evolution (3900-3600 Ma). Precambrian Research 78, 1-39.

Nutman, A.P., Bennett, V.C., Friend, C.R.L., Norman, M., 1999. Meta-igneous (non-gneissic) tonalites and quartz-diorites from an extensive ca. 3800 Ma terrain south of the Isua

supracrustal belt, southern West Greenland: constraints on early crust formation. Contributions to Mineralogy and Petrology 137, 364-388.

Nutman, A.P., Hagiya, H., Maruyama, S., 1995. SHRIMP U-Pb single zircon geochronology of a Proterozoic mafic dyke, Isukasia, southern West Greenland. Bulletin of the Geological Society of Denmark 42, 16-20.

Nutman, A.P., Friend, C.R.L., Bennett, V.C., McGregor, V.R., 2000. The early Archaean Itsaq Gneiss Complex of southern West Greenland: The importance of field observations in interpreting dates and isotopic data constraining early terrestrial evolution: Geochimica et Cosmochimica Acta 64, 3035-3060.

Nutman, A.P., Friend, C.R.L., Bennett, V.C., 2002. Evidence for 3650-3600 Ma assembly of the northern end of the Itsaq Gneiss Complex, Greenland. Implication for early Archean tectonics. Tectonics, **21**, article 5

Nutman, A.P., Friend, C.R.L., Barker, S.L.L., McGregor, V.R., 2004. Inventory and assessment of Palaeoarchaean gneiss terrains and detrital zircons in southern West Greenland. Precambrian Research 135, 281-314.

Nutman, A.P., Bennett, V.C., Friend, C.R.L., Horie, K., Hidaka, H., 2007. ~3850 Ma tonalites in the Nuuk region, Greenland: Geochemistry and their reworking within an Eoarchaean gneiss complex. Contributions to Mineralogy and Petrology 154, 385–408.

Nutman, A.P., Friend, C.R.L., Hiess, J., 2010. Setting of the ~2560 Ma Qôrqut granite complex in the Archaean crustal evolution of southern West Greenland. American Journal of Science 310, 1081-1114.

Nutman, A.P., Bennett, V.C., Friend, C.R.L., 2013a. The emergence of the Eoarchaean proto-arc: evolution of a c. 3700 Ma convergent plate boundary at Isua, West Greenland. In: Roberts, N.M.W., van Kranendonk, M., Parman, S., Shirey, S., Clift, P.D. (eds) Continent Formation Through Time. Geological Society, London, Special Publications, 389, article 5.

Nutman, A.P., Bennett, V.C., Friend, C.R.L., Hidaka, H., Yi, K., Lee, S.R., Kamiichi, T., 2013b. The Itsaq gneiss complex of Greenland: Episodic 3900 to 3600 Ma juvenile crust formation and recycling in the 3600 to 3600 Ma Isukasian orogeny. American Journal of Science, 213, 877-911.

Nutman, A.P., Friend, C.R.L., McGregor, V.R., Bennett, V.C., *in preparation*. Archaean crustal evolution of the Archaean craton of West Greenland: New map, isotopic data and synthesis.

Næraa, T., Scherstén, A., 2008. New zircon ages from the Tasiusarsuaq terrane, southern West Greenland. Geological Survey of Denmark and Greenland Bulletin 15, 73–76.

Næraa, T., Scherstén, A., Rosing, M.T., Kemp, A.I.S., Hoffmann, J.E., Kokfelt, T.F., Whitehouse, M.J., 2012. Hafnium isotope evidence for a transition in the dynamics of continental growth 3.2 Gyr ago. Nature 485, 627-630.

Patchett P.J., Kouvo O., Hedge C.E., Tatsumoto, M., 1981. Evolution of continental crust and mantle heterogeneity: evidence from Hf isotopes. Contributions to Mineralogy and Petrology 78, 279–297.

Polat, A., Hofmann, A.W., 2003. Alteration and geochemical patterns in the 3.7-3.8 Ga Isua greenstone belt, West Greenland. Precambrian Research 126, 197-218.

Polat, A., Appel, P.W.U., Frei, R., Pan, Y., Dilek, Y., Ordóñez-Calderón, J.C., Fryer, B., Hollis, J.A., Raith, J.G., 2007. Field and geochemical characteristics of the Mesoarchean (~3075Ma) Ivisaartoq greenstone belt, southern West Greenland: Evidence for seafloor hydrothermal alteration in supra-subduction oceanic crust. Gondwana Research 11, 69–91

Rasmussen, T.M., Thorning, L., 1999. Airborne geophysical survey in Greenland in 1998. Geology of Greenland Survey Bulletin 183, 34-38, Geological Survey of Denmark and Greenland, Copenhagen.

Rasmussen, T.M., van Gool, J.A.M., 2000. Aeromagnetic survey in southern West Greenland: project Aeromag 1999. Geology of Greenland Survey Bulletin 186, 73-77, Geological Survey of Denmark and Greenland, Copenhagen.

Rizo, H., Boyet, M., Blichert-Toft, J., and Rosing, M.T., 2011, Combined Nd and Hf isotope evidence for deep-seated source of Isua lavas. Earth and Planetary Science Letters, v. 312, p. 267-279.

Rosing, M.T., Nutman, A.P., Løfqvist, L., 2001. A new fragment of the early earth crust: the Aasivik terrane of West Greenland. Precambrian Research 105, 115-128.

Russell W.A., Papanastassiou D.A., Tombrello, T.A., 1978. Ca isotope fractionation on the Earth and other solar system material. Geochimica et Cosmochimica Acta 42, 1075–1090.

Scherer E., Munker C., Mezger K. 2001. Calibration of the lutetium–hafnium clock. Science 293, 683–687.

Schiøtte, L., Compston, W., and Bridgwater, D., 1989. U-Pb single-zircon age for the Tinissaq gneiss of southern West Greenland: A controversy resolved. Chemical Geology 79, 21-30.

Söderlund U., Patchett P.J., Vervoort J.D., Isachsen, C.E. 2004. The ^{176}Lu decay constant determined by Lu–Hf and U–Pb isotope systematics of Precambrian mafic intrusions. Earth and Planetary Science Letters 219, 311–324.

Thirlwall M.F., Anczkiewicz, R., 2004. Multidynamic isotope ratio analysis using MC–ICP–MS and the causes of secular drift in Hf, Nd and Pb isotope ratios. International Journal of Mass Spectrometry 235, 59–81.

Weis, D., Demaiffe, D., Souchez, R., Gow, A.J., Meese, D.A., 1997. Ice sheet development in Central Greenland: implications from the Nd, Sr and Pb isotopic compositions of basal material. Earth and Planetary Science Letters 150, 161-169.

Wells, P.R.A., 1976. Late Archean metamorphism in the Buksefjorden Region of southwest Greenland. Contributions to Mineralogy and Petrology 56, 229-242.

Windley, B.F., Garde, A.A., 2009. Arc-generated blocks with crustal sections in the North Atlantic craton of West Greenland: Crustal growth in the Archean with modern analogues. Earth Sciences Reviews 93, 1-30.

Williams, I.S., 1998. U-Th-Pb geochronology by ion microprobe. In Applications of microanalytical techniques to understanding mineralizing processes. In: M.A. McKibben, W.C.P. Shanks III and W.I. Ridley (Editors). Society of Economic Geology Short Course **7:** 1–35.

Woodhead, J., Hergt, J., 2005. A preliminary appraisal of seven natural zircon reference materials for in situ Hf isotope determination. Geostandards and Geoanalytical Research 29, 183–195.

Woodhead, J., Hergt, J., Shelley, M., Eggins, S., Kemp R., 2004. Zircon Hf-isotope analysis with an excimer laser, depth profiling, ablation of complex geometries, and concomitant age estimation. Chemical Geology 209, 121–135.

Vervoort, J.D., Patchett, P.J., Söderlund, U., Baker, M., 2004. Isotopic composition of Yb and the determination of Lu concentrations and Lu/Hf ratios by isotope dilution using MC-ICPMS. Geochemistry, Geophysics and Geosystems, 5, DOI: 10.1029/2004GC000721.

Figure Captions

Figure 1. (A) Archaean terrane map of the ice margin from East of Nuuk to Qarliit tasersuat, west Greenland. (B) Geological units and aeromagnetic signatures covering the same area. Inset in (A) shows the location in Greenland.

Figure 2. Cathodoluminescence images of representative zircons from Isua and eastern Ujaragssuit nunaat sand samples. $^{207}Pb/^{206}Pb$ ages and $\varepsilon Hf_{(t\text{-}zirc)}$ values are given with 2σ uncertainties.

Figure 3. Tera-Wasserburg $^{207}Pb/^{206}Pb$ versus $^{238}U/^{206}Pb$ concordia diagram for all 305 zircon analyses, excluding one Palaeoproterozoic grain. Analytical uncertainties are portrayed at the 2σ level.

Figure 4. Cumulate frequency distribution diagrams for ages of zircons. (A) Isua sand samples #1-3 and (B) eastern Ujaragssuit nunaat sand sample #4. (C) zircon age determinations for rocks in the northern part of the Tasiusarsuaq terrane, the Tuno terrane + the Qarliit nunaat assemblage, the Akia+Kapisilik terranes, the Tre Brødre terrane and the northern part of the Itsaq gneiss complex (Isukasia terrane) (data from Kinny, 1987; Schiøtte et al., 1989; Nutman et al., 1996, 1997, 1999, 2000, 2007; Crowley et al., 2002; Crowley, 2002, 2003; Friend and Nutman, 2005a,b; Garde et al., 2001; Garde, 2007; Næraa and Scherstén, 2008; Hiess et al., 2009; Horie et al., 2010; Nutman and McGregor, unpublished data). For the detrital zircon data in (A) and (B) the analyses with >5% difference between the $^{207}Pb/^{206}Pb$ and the $^{238}U/^{206}Pb$ ages were not plotted. Plot (C) was constructed from weighted mean $^{207}Pb/^{206}Pb$ ages of close to concordant zircon analyses, and thus are based on >2000 zircon analyses.

Figure 5. (A) zircon Th/U and (B) $\varepsilon Hf_{(t\text{-}zirc)}$ versus $^{207}Pb/^{206}Pb$ age plots.

Table captions.

Table 1. SHRIMP U-Th-Pb zircon data.

Table 2. LA-ICP-MS Hf isotopic data.

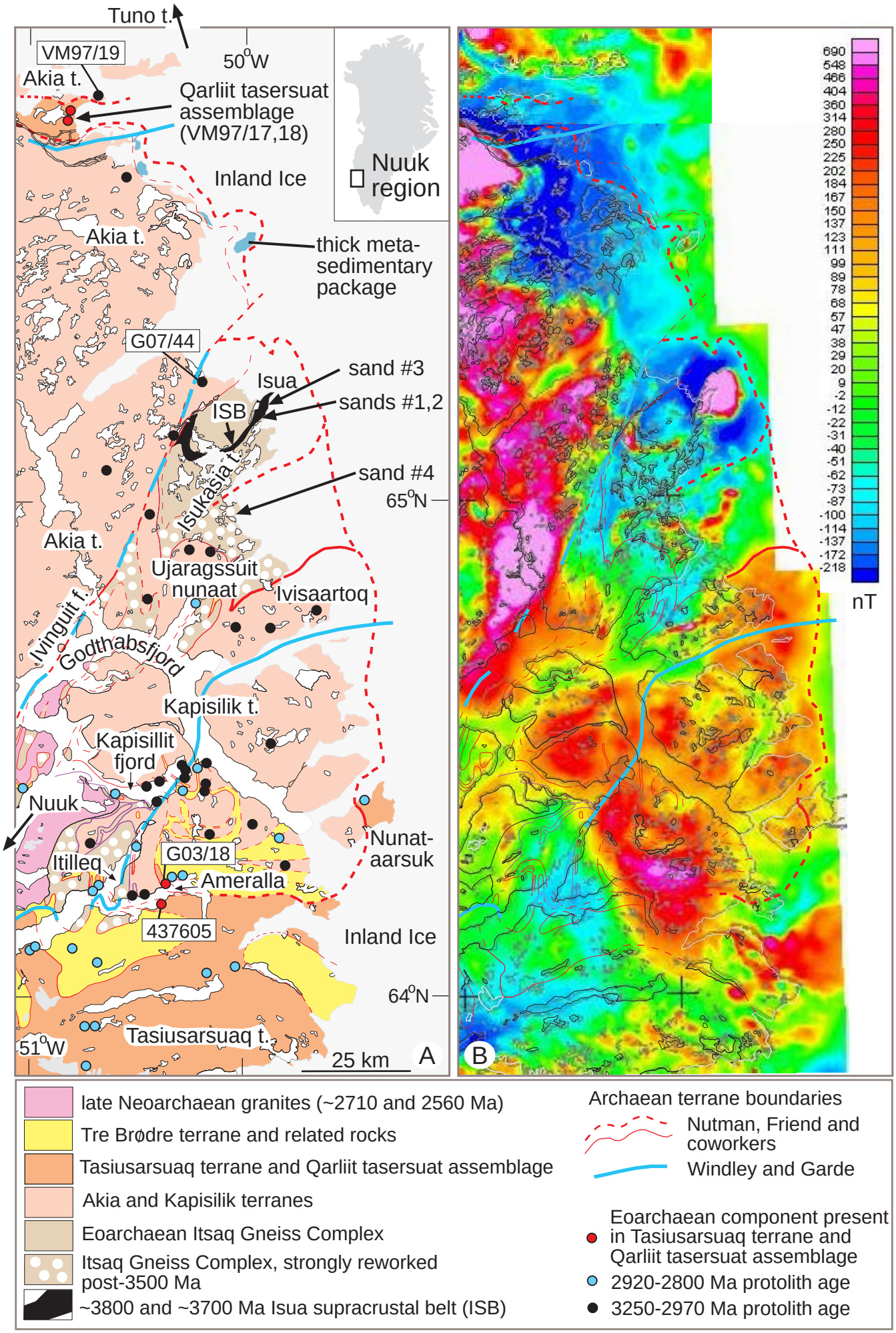
Tuno t.
VM97/19
Akia t.
50°W
Qarliit tasersuat assemblage (VM97/17,18)
Inland Ice
Nuuk region
Akia t.
thick meta-sedimentary package
G07/44
Isua
sand #3
sands #1,2
ISB
sand #4
Isukasia t.
65°N
Akia t.
Ujaragssuit nunaat
Ivisaartoq
Ivinguit f.
Godthabsfjord
Kapisilik t.
Kapisillit fjord
Nuuk
Nunat-aarsuk
Itilleq
G03/18
Ameralla
437605
Inland Ice
64°N
Tasiusarsuaq t.
51°W
25 km
A
B
690
548
466
404
360
314
280
250
225
202
184
167
150
137
123
111
99
89
78
68
57
47
38
29
20
9
-2
-12
-22
-31
-40
-51
-62
-73
-87
-100
-114
-137
-172
-218
nT
late Neoarchaean granites (~2710 and 2560 Ma)
Tre Brødre terrane and related rocks
Tasiusarsuaq terrane and Qarliit tasersuat assemblage
Akia and Kapisilik terranes
Eoarchaean Itsaq Gneiss Complex
Itsaq Gneiss Complex, strongly reworked post-3500 Ma
~3800 and ~3700 Ma Isua supracrustal belt (ISB)
Archaean terrane boundaries
Nutman, Friend and coworkers
Windley and Garde
Eoarchaean component present in Tasiusarsuaq terrane and Qarliit tasersuat assemblage
2920-2800 Ma protolith age
3250-2970 Ma protolith age

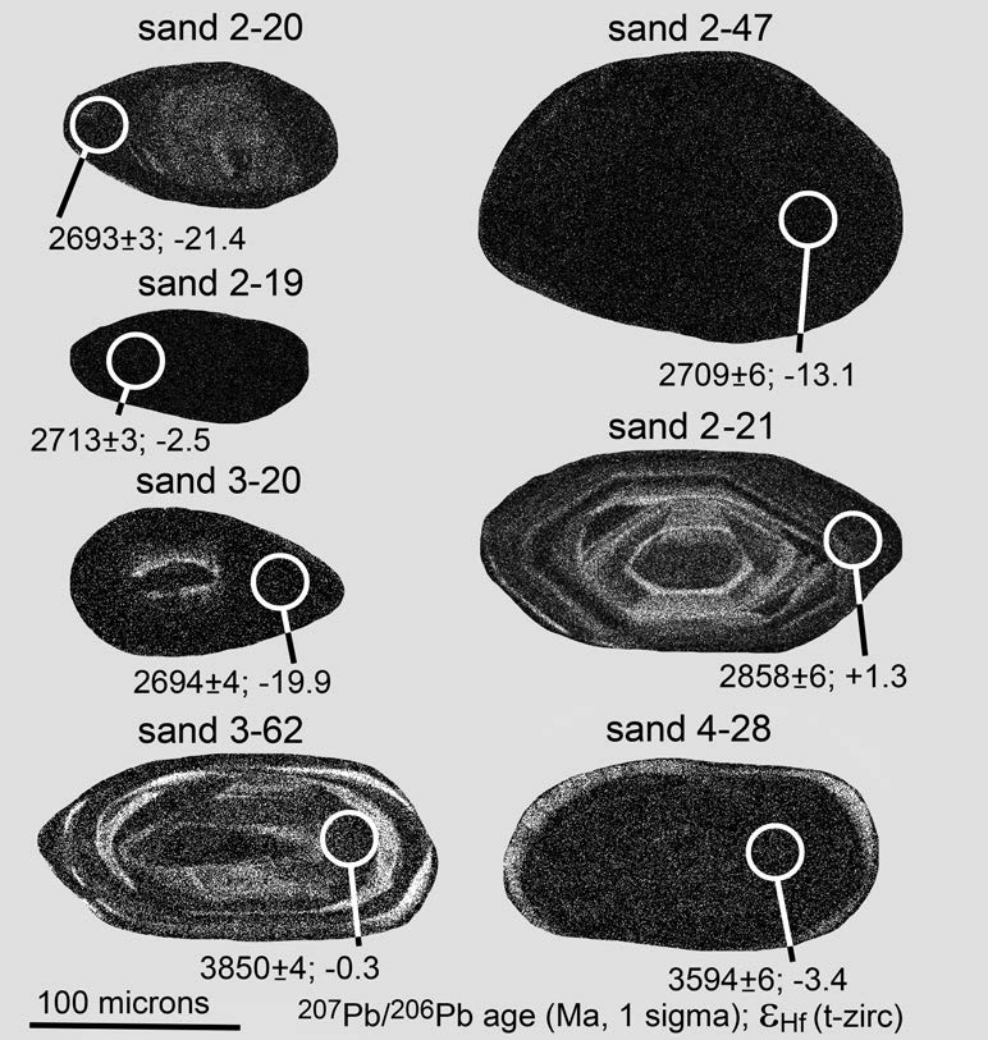
sand 2-20
2693±3; -21.4
sand 2-47
2709±6; -13.1
sand 2-19
2713±3; -2.5
sand 2-21
2858±6; +1.3
sand 3-20
2694±4; -19.9
sand 3-62
3850±4; -0.3
sand 4-28
3594±6; -3.4
100 microns
$^{207}Pb/^{206}Pb$ age (Ma, 1 sigma); ε_{Hf} (t-zirc)

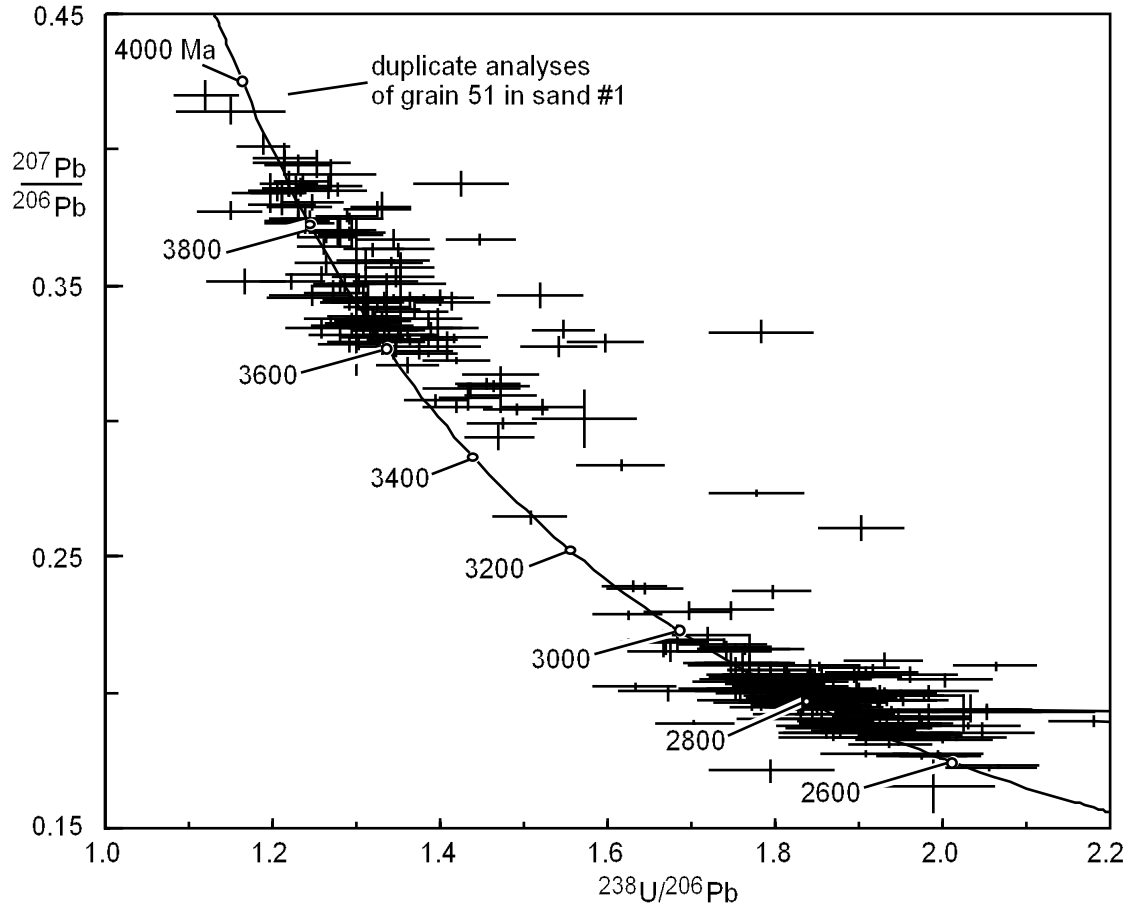
0.45
0.35
0.25
0.15
$^{207}Pb/^{206}Pb$
4000 Ma
duplicate analyses
of grain 51 in sand #1
3800
3600
3400
3200
3000
2800
2600
1.0
1.2
1.4
1.6
1.8
2.0
2.2
$^{238}U/^{206}Pb$

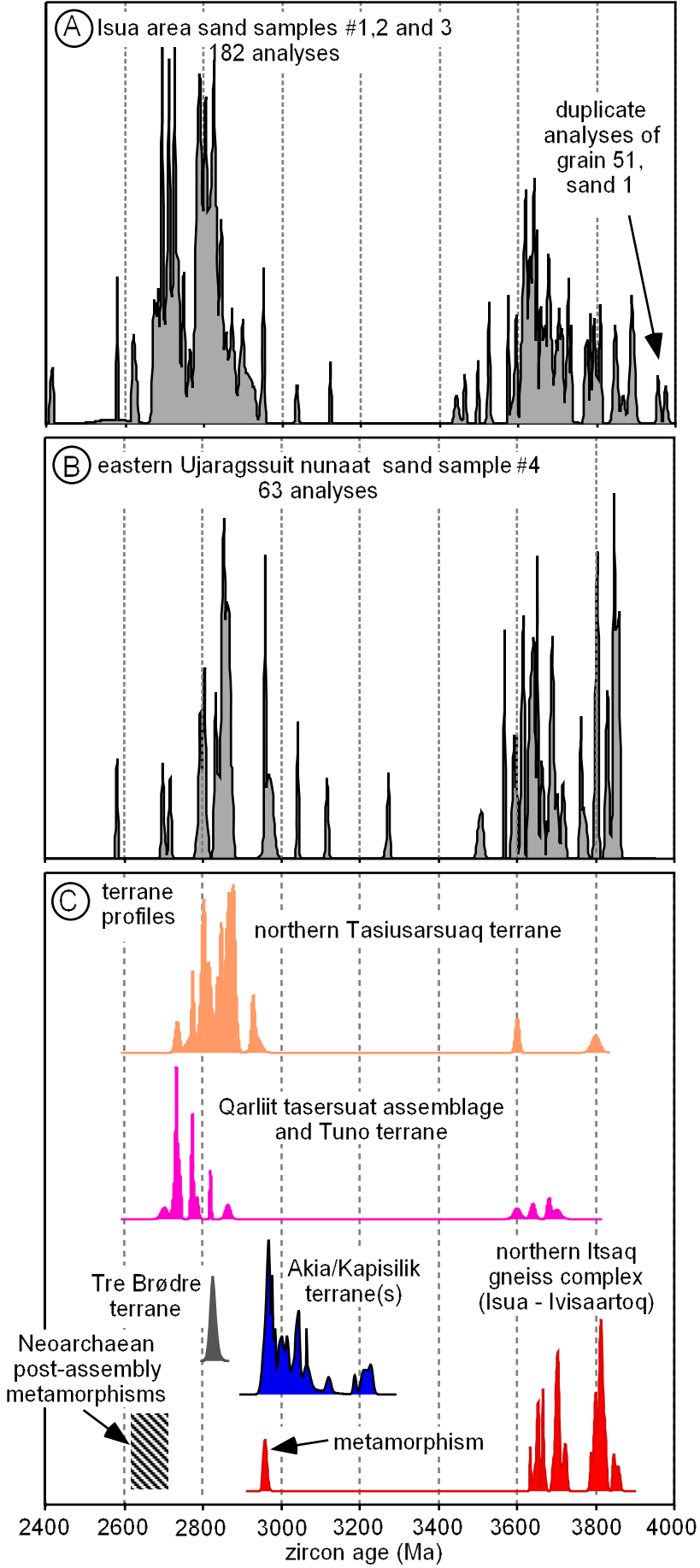
A
Isua area sand samples #1,2 and 3
182 analyses
duplicate analyses of grain 51, sand 1
B
eastern Ujaragssuit nunaat sand sample #4
63 analyses
C
terrane profiles
northern Tasiusarsuaq terrane
Qarliit tasersuat assemblage and Tuno terrane
Tre Brødre terrane
Akia/Kapisilik terrane(s)
northern Itsaq gneiss complex (Isua - Ivisaartoq)
Neoarchaean post-assembly metamorphisms
metamorphism
2400
2600
2800
3000
3200
3400
3600
3800
4000
zircon age (Ma)

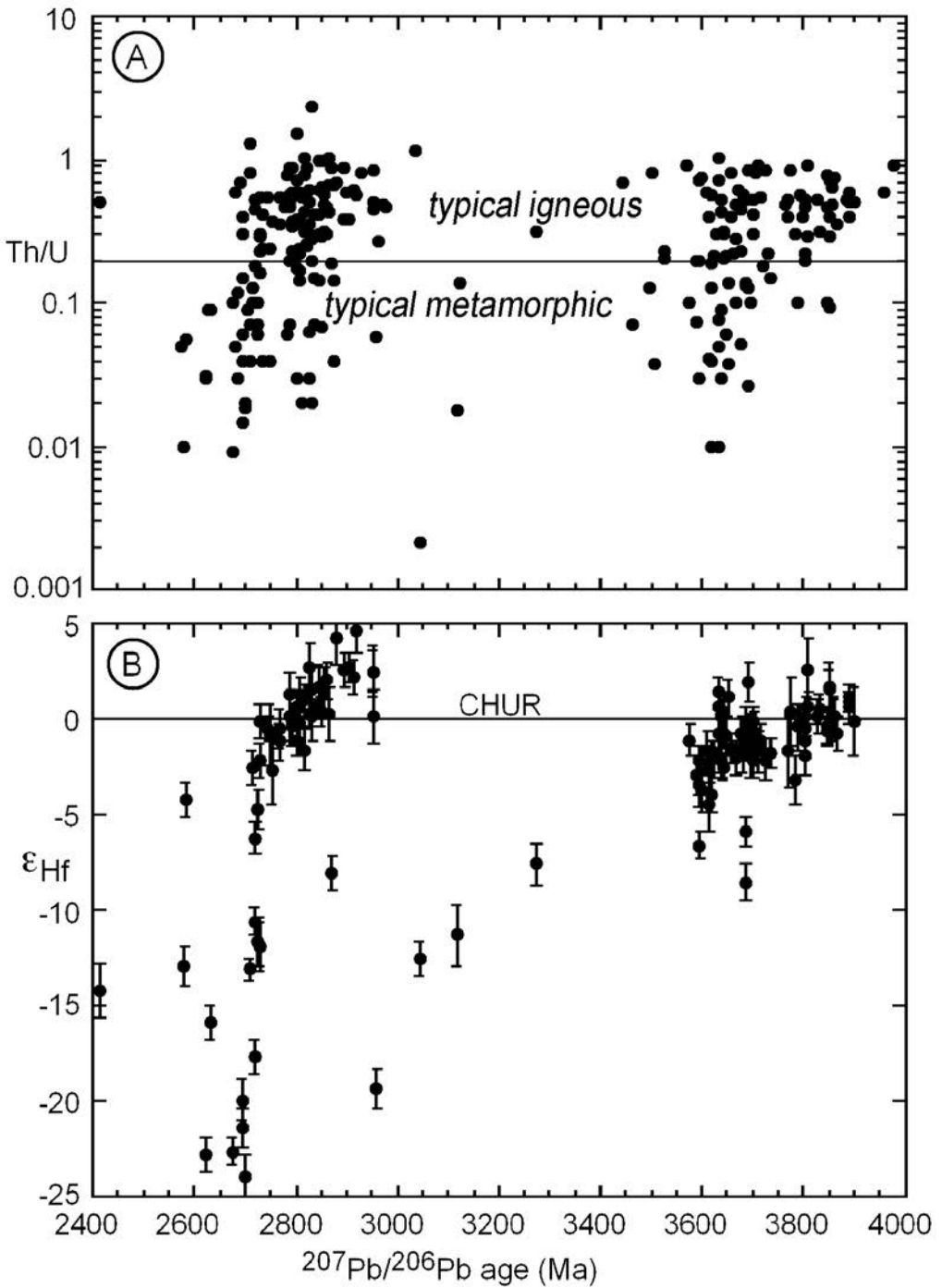
A
10
1
0.1
0.01
0.001
Th/U
typical igneous
typical metamorphic
B
5
0
-5
-10
-15
-20
-25
εHf
CHUR
2400
2600
2800
3000
3200
3400
3600
3800
4000
207Pb/206Pb age (Ma)

Table 1: SHRIMP U-Th-Pb zircon analyses

Site	Grain/site type	U ppm	Th ppm	Th/U	comm. ^{206}Pb%	^{238}U/^{206}Pb* ratio	^{207}Pb/^{206}Pb* ratio	^{207}Pb/^{206}Pb* site date (Ma)	conc (%)	εHf (t-zircon)	2SD
Sand samples											
sand #1 (Isua: 65°9.25'N 49°49.85'W - WGS84 datum)											
1.1	e,h,eq	181	154	0.848	0.057	1.861 ± 0.025	0.1864 ± 0.0009	2711 ± 8	103		
2.1	e,osc,p	214	48	0.223	0.185	1.845 ± 0.024	0.2006 ± 0.0009	2831 ± 8	98		
3.1	e,h,p	2596	90	0.035	0.006	1.918 ± 0.022	0.1836 ± 0.0002	2686 ± 2	101		
4.1	e,osc,p	429	133	0.311	0.022	1.263 ± 0.016	0.3680 ± 0.0007	3783 ± 3	99	-3.2	1.3
5.1	e,osc/h,p	587	170	0.290	0.016	1.315 ± 0.016	0.3355 ± 0.0007	3642 ± 3	100	0.4	0.9
6.1	e,osc/h,p	120	26	0.217	0.026	1.376 ± 0.020	0.3253 ± 0.0013	3595 ± 6	97	-6.6	0.7
7.1	e,osc/h,p	365	166	0.455	0.039	1.196 ± 0.015	0.3972 ± 0.0016	3898 ± 6	101	-1.4	1.7
7.1	duplicate Hf									-0.1	1.8
7.2	e,osc/h,p	240	30	0.126	0.058	1.341 ± 0.019	0.3475 ± 0.0011	3696 ± 5	103		
8.1	e,osc/h,p	217	133	0.614	0.023	1.292 ± 0.017	0.3284 ± 0.0010	3610 ± 5	98	-1.7	1.1
9.1	e,osc/h,p	163	18	0.108	0.085	1.280 ± 0.018	0.3688 ± 0.0025	3786 ± 10	95	-0.4	1.2
10.1	m,hd,p	416	9	0.022	0.154	1.913 ± 0.028	0.2010 ± 0.0012	2834 ± 9	100		
11.1	c,osc,p	237	112	0.474	0.092	1.851 ± 0.024	0.1956 ± 0.0008	2790 ± 7	101		
12.1	e,hd,p	1294	81	0.062	0.196	1.306 ± 0.015	0.3368 ± 0.0005	3648 ± 2	101	-0.9	0.9
13.1	e,hd,p	231	83	0.361	0.432	1.907 ± 0.048	0.1847 ± 0.0010	2696 ± 9	99		
14.1	e,osc,p	137	113	0.823	0.089	1.319 ± 0.019	0.3384 ± 0.0013	3656 ± 6	101	-1.5	0.8
15.1	m,hd,p	1952	110	0.056	0.012	1.833 ± 0.021	0.1946 ± 0.0011	2781 ± 10	100		
16.1	e,osc/h,p	679	302	0.445	0.038	1.260 ± 0.015	0.3650 ± 0.0006	3771 ± 2	101	-1.7	1.9
17.1	e,hd,p	1465	59	0.040	0.033	1.872 ± 0.022	0.1894 ± 0.0004	2737 ± 3	102		
18.1	e,osc/h,p	162	41	0.251	bld	1.758 ± 0.024	0.2026 ± 0.0010	2847 ± 8	98		
19.1	e,osc,p	135	40	0.293	0.025	1.819 ± 0.026	0.2041 ± 0.0011	2859 ± 9	98		
20.1	m,osc,p	321	13	0.040	0.020	1.814 ± 0.023	0.2060 ± 0.0016	2874 ± 13	90		
21.1	e,rex,p	1062	298	0.281	0.184	2.119 ± 0.025	0.1865 ± 0.0004	2711 ± 4	102		
22.1	e,osc/h,p	233	92	0.395	0.005	1.303 ± 0.017	0.3291 ± 0.0010	3613 ± 5	95	-2.6	0.7
23.1	r,hd,p	358	60	0.167	0.179	1.936 ± 0.024	0.1954 ± 0.0007	2788 ± 6	94		
24.1	e,hd,p	279	36	0.127	0.006	1.951 ± 0.025	0.1990 ± 0.0007	2818 ± 6	103		
25.1	e,osc,p	300	177	0.588	0.715	1.886 ± 0.030	0.1833 ± 0.0021	2683 ± 9	100		
26.1	e,osc,p	515	253	0.492	0.073	1.818 ± 0.022	0.2003 ± 0.0006	2829 ± 5	100		
27.1	e,osc,p	556	22	0.040	0.015	1.324 ± 0.016	0.3303 ± 0.0014	3619 ± 6	91	-3.9	0.9
28.1	e,hd,p	461	81	0.176	0.084	2.058 ± 0.025	0.1925 ± 0.0006	2764 ± 5	100		
29.1	e,hd,p	1387	121	0.087	0.001	1.924 ± 0.023	0.1860 ± 0.0003	2707 ± 3	98		
30.1	m,osc,p	65	29	0.442	bld	1.276 ± 0.022	0.3712 ± 0.0020	3796 ± 8	101		

31.1	e,osc,p	261	88	0.338	0.183	1.799 ± 0.024	0.2002 ± 0.0009	2828 ± 8	102		
32.1	e,osc,p,fr	392	54	0.139	0.010	1.205 ± 0.015	0.3837 ± 0.0015	3846 ± 6	100	-0.6	0.8
33.1	e,h,p	441	56	0.128	0.005	1.935 ± 0.024	0.1824 ± 0.0006	2675 ± 6	103		
34.1	e,hd,p	1731	82	0.047	10.545	1.977 ± 0.032	0.1715 ± 0.0075	2573 ± 73	93		
35.1	e,hd,p	2837	1498	0.528	0.068	1.492 ± 0.018	0.3032 ± 0.0003	3487 ± 2	102		
36.1	e,osc/h,p,fr	146	98	0.672	0.156	1.901 ± 0.027	0.1841 ± 0.0012	2690 ± 11	99		
37.1	e,hd,p	1018	115	0.113	0.004	1.937 ± 0.025	0.1869 ± 0.0004	2715 ± 4	103		
38.1	e,osc/h,p	164	54	0.330	0.188	1.862 ± 0.026	0.1848 ± 0.0011	2696 ± 10	101		
39.1	e,osc,p	146	127	0.870	bld	1.227 ± 0.018	0.3744 ± 0.0013	3809 ± 5	90	0.6	0.8
40.1	e,h,p	2188	298	0.136	0.010	1.927 ± 0.023	0.2136 ± 0.0009	2933 ± 7	101		
41.1	e,hd,p	746	11	0.015	0.016	1.818 ± 0.022	0.1981 ± 0.0005	2810 ± 4	101		
42.1	e,hd,p	3642	135	0.037	0.001	1.894 ± 0.024	0.1865 ± 0.0002	2712 ± 2	98		
43.1	e,hd,p	788	17	0.021	0.029	1.967 ± 0.024	0.1854 ± 0.0005	2702 ± 4	92		
44.1	e,hd,p	637	45	0.070	0.581	2.034 ± 0.106	0.1940 ± 0.0024	2776 ± 20	93		
45.1	e,h/rex,p	236	60	0.254	0.175	1.429 ± 0.019	0.3281 ± 0.0011	3608 ± 5	98		
46.1	r,hd,p	1072	45	0.042	0.010	1.916 ± 0.023	0.1910 ± 0.0004	2750 ± 4	100		
47.1	e,hd,p	1831	133	0.073	0.030	1.906 ± 0.036	0.1863 ± 0.0004	2710 ± 3	95		
48.1	e,rex,p	277	62	0.223	0.229	1.415 ± 0.019	0.3239 ± 0.0025	3589 ± 12	100		
49.1	e,osc/h,p	107	41	0.387	0.012	1.309 ± 0.020	0.3392 ± 0.0016	3659 ± 7	93		
50.1	e,hd,p	592	77	0.130	0.084	2.032 ± 0.077	0.1906 ± 0.0031	2748 ± 27	103		
51.1	e,osc/h,p	210	136	0.648	0.047	1.151 ± 0.030	0.4132 ± 0.0013	3958 ± 8	96		
51.2	m,osc,h,p	73	65	0.892	0.042	1.122 ± 0.018	0.4184 ± 0.0021	3976 ± 8	110		
52.1	e,hd,p	583	17	0.030	0.208	1.900 ± 0.042	0.2001 ± 0.0025	2827 ± 2	99		
53.1	e,hd/rex,p,fr	855	260	0.304	0.015	1.631 ± 0.023	0.2034 ± 0.0003	2854 ± 3	87		
54.1	e,osc/h,p	494	168	0.340	0.024	1.916 ± 0.055	0.1886 ± 0.0022	2730 ± 19	97		
55.1	e,rex,p	146	34	0.231	0.051	1.546 ± 0.022	0.3248 ± 0.0017	3593 ± 8	98		
56.1	e,osc/h,p	556	28	0.051	0.009	2.002 ± 0.029	0.1828 ± 0.0003	2679 ± 3	98		
57.1	e,osc/h,p	112	53	0.474	0.037	1.765 ± 0.026	0.2159 ± 0.0008	2951 ± 6	98	2.5	1.3
58.1	e,h,p	555	124	0.223	0.039	1.875 ± 0.025	0.1965 ± 0.0004	2797 ± 3	96		
59.1	e,osc/h,p,fr	58	33	0.565	0.049	1.872 ± 0.030	0.1972 ± 0.0010	2803 ± 9	94		
60.1	e,osc,p	106	46	0.429	0.008	1.253 ± 0.019	0.3945 ± 0.0023	3888 ± 9	99	1.1	0.7
60.1	2nd spot									0.6	0.8
60.2	m,osc,p	144	65	0.453	0.005	1.217 ± 0.018	0.3951 ± 0.0022	3891 ± 8	94		
61.1	e,h/rex.p	575	388	0.675	0.027	1.463 ± 0.020	0.3128 ± 0.0004	3535 ± 2	96		
62.1	e,hd,p	350	5	0.015	0.014	1.335 ± 0.018	0.3331 ± 0.0010	3631 ± 4	100	0.7	0.7
63.1	e,osc/h,p	162	46	0.282	0.024	1.900 ± 0.027	0.2041 ± 0.0011	2859 ± 8	99		
64.1	e,hd,p	844	47	0.056	0.144	1.981 ± 0.028	0.1882 ± 0.0003	2727 ± 2	86		
65.1	e,hd,p,fr	321	24	0.075	0.006	1.851 ± 0.025	0.1956 ± 0.0005	2790 ± 4	98		
66.1	e,osc/h,p	183	20	0.112	0.052	1.312 ± 0.024	0.3409 ± 0.0032	3667 ± 14	92	-2.0	0.9

67.1	m,osc/h,p	194	156	0.803	0.063	1.414 ± 0.025	0.3937 ± 0.0016	3885 ± 6	94		
68.1	m,osc/h,p	138	124	0.899	0.030	1.315 ± 0.019	0.3509 ± 0.0009	3711 ± 4	99	-1.7	1.1
69.1	m,osc/rex,p	78	33	0.422	0.102	1.419 ± 0.022	0.3409 ± 0.0012	3667 ± 5	100		
70.1	e,h,p	396	196	0.495	0.035	1.494 ± 0.020	0.2968 ± 0.0005	3454 ± 3	99		
71.1	e,osc,p	55	54	0.994	0.037	1.820 ± 0.030	0.2022 ± 0.0012	2844 ± 10	96		
72.1	e,hb/rex,p	59	13	0.225	0.037	1.240 ± 0.021	0.3728 ± 0.0025	3803 ± 10	104	-1.1	0.9
73.1	m,hd,p	1139	68	0.059	0.005	1.953 ± 0.026	0.1848 ± 0.0003	2697 ± 2	99		

sand #2 (Isua: 65°9.25'N 49°49.85'W - WGS84 datum)

1.1	r,h,eq	227	50	0.221	0.037	1.337 ± 0.019	0.3395 ± 0.0014	3661 ± 6	98		
2.1	m,h,p	84	48	0.574	bld	1.783 ± 0.030	0.3302 ± 0.0016	3618 ± 7	74		
3.1	e,hd,p	944	87	0.092	0.043	2.031 ± 0.031	0.1884 ± 0.0004	2728 ± 3	94		
4.1	m,osc,p	42	17	0.408	0.022	1.167 ± 0.023	0.3529 ± 0.0018	3720 ± 8	110		
5.1	m,osc,eq	105	57	0.538	0.010	1.223 ± 0.019	0.3521 ± 0.0010	3716 ± 4	105	-1.1	0.8
6.1	e,h,p	886	114	0.129	0.255	1.360 ± 0.018	0.3304 ± 0.0004	3619 ± 2	97	-1.7	0.6
7.1	m,h,p	943	149	0.158	0.006	1.884 ± 0.027	0.1885 ± 0.0003	2729 ± 2	101	-11.9	1.3
8.1	e,osc,p	146	85	0.583	0.033	1.231 ± 0.019	0.3707 ± 0.0010	3794 ± 4	100	-0.2	1.0
10.1	m,hd,p	1592	51	0.032	0.015	1.704 ± 0.023	0.1892 ± 0.0002	2735 ± 2	111		
11.1	e,osc/rex,p	105	22	0.214	0.112	1.350 ± 0.021	0.3634 ± 0.0011	3764 ± 4	93		
12.1	m,rex,p	249	31	0.126	0.017	1.420 ± 0.020	0.3056 ± 0.0007	3499 ± 3	98		
13.1	m,osc,p,fr	150	133	0.889	0.079	1.815 ± 0.029	0.1997 ± 0.0007	2823 ± 5	100		
14.1	m,osc,p,fr	83	35	0.419	0.040	1.257 ± 0.020	0.3490 ± 0.0011	3702 ± 5	102	-0.6	1.0
15.1	e,rex,eq	61	25	0.411	0.010	1.673 ± 0.029	0.2006 ± 0.0011	2831 ± 9	108		
16.1	e,osc,p	58	41	0.711	0.021	1.772 ± 0.032	0.1971 ± 0.0011	2803 ± 9	104		
17.1	m,osc,p	262	49	0.187	0.005	1.762 ± 0.025	0.2055 ± 0.0005	2871 ± 4	101	-8.1	0.9
18.1	c,osc,p	89	18	0.199	0.129	1.836 ± 0.029	0.1951 ± 0.0009	2786 ± 8	100		
19.1	e,hd,p	884	113	0.128	0.091	1.917 ± 0.026	0.1867 ± 0.0003	2713 ± 3	100	-2.5	0.9
20.1	r,hd,p	924	40	0.043	0.175	1.969 ± 0.026	0.1848 ± 0.0003	2696 ± 3	98	-21.4	1.0
21.1	e,osc,p	141	45	0.318	0.012	1.811 ± 0.027	0.2039 ± 0.0007	2858 ± 6	99	1.3	0.8
22.1	m,h/rex,p	141	100	0.714	0.183	1.346 ± 0.021	0.3251 ± 0.0009	3594 ± 4	99	-2.1	0.7
23.1	e,osc,p,fr	308	51	0.165	0.101	1.448 ± 0.020	0.3672 ± 0.0006	3780 ± 2	87		
24.1	e,osc,p	59	5	0.093	bld	1.258 ± 0.021	0.3344 ± 0.0014	3637 ± 6	105		
25.1	m,osc,eq	91	208	2.298	0.071	1.521 ± 0.025	0.2010 ± 0.0009	2834 ± 7	100	0.2	1.4
26.1	e,h,p	155	44	0.284	0.010	1.369 ± 0.020	0.3411 ± 0.0009	3668 ± 4	95		
27.1	e,hd,p	1047	29	0.028	0.006	1.330 ± 0.018	0.3349 ± 0.0003	3640 ± 1	99	-2.1	0.9
28.1	e,osc/h,p	520	25	0.047	0.081	1.382 ± 0.019	0.3433 ± 0.0005	3678 ± 2	94		
29.1	e,h,p	518	301	0.582	0.098	1.364 ± 0.019	0.3297 ± 0.0005	3616 ± 2	97		
30.1	e,osc,p	113	67	0.588	0.033	1.215 ± 0.019	0.3956 ± 0.0019	3892 ± 7	99	0.9	0.9
30.2	e,osc,p	114	61	0.533	0.018	1.230 ± 0.019	0.3939 ± 0.0011	3886 ± 4	98		

31.1	e,h,p	79	12	0.153	0.088	1.871 ± 0.030	0.1846 ± 0.0009	2695 ± 8	103			
31.2	e,hb,p	11	3	0.242	0.195	1.858 ± 0.051	0.1892 ± 0.0028	2735 ± 24	102			
32.1	m,osc,eq	42	20	0.467	bld	1.196 ± 0.022	0.3842 ± 0.0033	3848 ± 13	103	-0.6	0.8	
33.1	m,hd,p	668	45	0.068	0.013	1.474 ± 0.020	0.2990 ± 0.0010	3465 ± 5	95			
34.1	e,hd/rex,p	73	64	0.875	0.184	1.947 ± 0.034	0.1952 ± 0.0010	2786 ± 9	95			
35.1	e,hd,p	2243	72	0.032	0.002	1.976 ± 0.026	0.1766 ± 0.0002	2621 ± 2	101			
36.1	r,hd,p	1646	17	0.010	0.002	1.319 ± 0.017	0.3307 ± 0.0010	3620 ± 5	101			
37.1	e,osc,eq	146	288	1.975	0.159	2.429 ± 0.044	0.3739 ± 0.0013	3807 ± 5	43			
38.1	e,h,p	107	48	0.447	0.435	1.301 ± 0.020	0.3433 ± 0.0011	3677 ± 5	100	-1.5	0.7	
39.1	e,hb/rex,p	16	1	0.049	0.187	1.353 ± 0.031	0.3330 ± 0.0025	3631 ± 12	98	1.4	0.8	
40.1	e,osc,p,fr	179	104	0.580	0.026	1.363 ± 0.020	0.3436 ± 0.0008	3679 ± 3	95	-1.9	0.9	
41.1	e,hd/rex,p	576	174	0.301	0.059	1.385 ± 0.020	0.3321 ± 0.0004	3627 ± 2	95			
42.1	m,osc,p	103	62	0.600	bld	1.842 ± 0.029	0.2092 ± 0.0008	2899 ± 6	95			
43.1	m,rex,p	231	143	0.620	0.016	1.325 ± 0.020	0.3425 ± 0.0007	3674 ± 3	98			
44.1	e,osc,p	135	53	0.391	0.099	1.770 ± 0.027	0.2089 ± 0.0013	2897 ± 10	99	2.6	0.9	
45.1	e,osc,p	94	20	0.213	0.024	1.349 ± 0.021	0.3314 ± 0.0010	3623 ± 5	98	-2.0	0.8	
46.1	e,hd,p	1730	162	0.093	0.001	1.908 ± 0.025	0.1771 ± 0.0002	2626 ± 2	104			
47.1	e,hd,p	153	198	1.296	0.022	1.933 ± 0.032	0.1862 ± 0.0007	2709 ± 6	99	-13.1	0.6	
48.1	m,osc,p	203	31	0.151	0.026	1.341 ± 0.019	0.3567 ± 0.0007	3736 ± 3	95	-1.8	0.8	
49.1	e,osc,p	207	84	0.405	0.003	1.789 ± 0.026	0.2022 ± 0.0006	2844 ± 5	101			
50.1	e,osc,eq	75	20	0.265	0.030	1.343 ± 0.022	0.3676 ± 0.0014	3781 ± 6	93			
51.1	m,hd,p	1360	122	0.090	0.002	1.996 ± 0.027	0.1776 ± 0.0002	2630 ± 2	99	-15.8	0.9	
52.1	r,h,p	285	39	0.135	0.064	1.273 ± 0.018	0.3452 ± 0.0020	3686 ± 9	102			
53.1	e,osc/h,p	527	51	0.096	0.014	1.420 ± 0.019	0.3212 ± 0.0004	3575 ± 2	95	-1.1	0.8	
54.1	m,hd/rex,p	159	86	0.542	0.114	1.472 ± 0.022	0.3166 ± 0.0008	3553 ± 4	92			
55.1	e,osc/rex,p	639	183	0.287	0.026	1.289 ± 0.018	0.3745 ± 0.0010	3810 ± 4	96			
56.1	e,hd,p	548	41	0.075	0.017	1.916 ± 0.026	0.1882 ± 0.0008	2727 ± 7	99	-11.6	1.3	
57.1	e,osc,p	233	83	0.356	0.161	1.940 ± 0.028	0.1927 ± 0.0006	2766 ± 5	96	-0.5	1.0	
58.1	e,osc,p	110	66	0.598	0.107	1.931 ± 0.031	0.1958 ± 0.0008	2791 ± 7	95			
59.1	e,hd,p	789	153	0.194	0.272	1.416 ± 0.019	0.3278 ± 0.0004	3607 ± 2	94			
60.1	m,hd,p	1157	78	0.067	0.013	1.779 ± 0.028	0.2728 ± 0.0003	3322 ± 2	83			
61.1	e,osc,p	179	96	0.534	0.084	1.334 ± 0.020	0.3452 ± 0.0008	3686 ± 4	97	-0.3	1.0	
62.1	e,osc,p	815	332	0.408	0.023	1.869 ± 0.026	0.2014 ± 0.0003	2837 ± 2	97			
63.1	m,hd/rex,p	166	132	0.796	0.289	1.523 ± 0.024	0.3059 ± 0.0009	3500 ± 4	91			
64.1	e,osc,p	227	96	0.422	1.235	1.973 ± 0.029	0.1894 ± 0.0012	2737 ± 11	96			
65.1	e,osc,p	167	69	0.411	0.056	1.324 ± 0.020	0.3763 ± 0.0009	3817 ± 4	93			
66.1	m,osc,p	175	37	0.209	0.010	1.332 ± 0.019	0.3365 ± 0.0008	3647 ± 4	99	-0.9	1.0	
67.1	c,osc,p	476	400	0.841	0.013	1.292 ± 0.019	0.3660 ± 0.0005	3775 ± 2	97	0.3	1.9	
67.1	duplicate Hf									0.4	1.8	

68.1	e,rex,p	266	234	0.880	0.098	1.927 ± 0.030	0.1959 ± 0.0005	2793 ± 4	95		
69.1	m,hd,p	655	78	0.119	0.124	2.019 ± 0.029	0.1835 ± 0.0003	2685 ± 3	96		
70.1	m,rex,p	1094	153	0.140	0.020	1.644 ± 0.022	0.2408 ± 0.0003	3125 ± 2	98		
71.1	e,hd,p	1155	214	0.185	0.003	1.932 ± 0.026	0.1873 ± 0.0002	2719 ± 2	99	-17.7	0.9
72.1	m,osc,p	113	63	0.553	bld	1.149 ± 0.019	0.3782 ± 0.0012	3825 ± 5	108		
73.1	e,hd,p,fr	1917	14	0.007	0.013	2.057 ± 0.027	0.1723 ± 0.0002	2580 ± 2	99	-12.9	1.0
74.1	m,rex,p	286	297	1.038	0.554	1.572 ± 0.030	0.3019 ± 0.0019	3480 ± 10	89		
75.1	e,osc,p	135	111	0.827	0.027	1.349 ± 0.021	0.3541 ± 0.0009	3725 ± 4	95	-2.1	1.1

sand #3 (Isua: 65°11.55'N 49°48.07'W - WGS84 datum)

1.1	e,osc,p	482	109	0.227	0.059	1.928 ± 0.024	0.1886 ± 0.0006	2730 ± 5	98		
2.1	e,osc,p	203	92	0.455	0.076	1.730 ± 0.024	0.2161 ± 0.0010	2952 ± 7	100	2.5	1.1
3.1	e,osc,p	261	47	0.179	0.053	1.957 ± 0.026	0.1957 ± 0.0009	2791 ± 7	94		
4.1	e,osc,p	352	291	0.825	0.020	1.288 ± 0.017	0.3497 ± 0.0009	3706 ± 4	100	-0.9	0.9
5.1	e,osc,p	106	50	0.468	0.098	1.835 ± 0.029	0.1953 ± 0.0023	2788 ± 19	101	1.3	1.1
6.1	e,rex,p	102	26	0.260	0.056	1.831 ± 0.046	0.1994 ± 0.0012	2821 ± 10	99		
7.1	e,osc,p	177	184	1.038	0.045	1.811 ± 0.025	0.1988 ± 0.0009	2817 ± 8	101	-1.6	1.1
8.1	m,rex,p,fr	410	178	0.433	0.089	1.828 ± 0.024	0.1990 ± 0.0008	2818 ± 6	100		
9.1	e,rex/h,p	287	69	0.240	0.066	1.749 ± 0.024	0.2303 ± 0.0010	3054 ± 7	94		
10.1	e,h,p	249	116	0.466	0.062	1.851 ± 0.026	0.1943 ± 0.0010	2779 ± 8	100		
11.1	m,hb/rex,p	51	2	0.037	0.146	1.797 ± 0.037	0.1712 ± 0.0021	2569 ± 21	114		
12.1	m,osc,p	176	123	0.699	0.069	1.757 ± 0.026	0.2067 ± 0.0012	2880 ± 10	101	4.2	1.4
13.1	m,osc,p	213	172	0.808	0.136	1.681 ± 0.024	0.2132 ± 0.0011	2930 ± 9	103		
14.1	e,hd,p	956	233	0.244	0.179	1.936 ± 0.024	0.1907 ± 0.0006	2748 ± 5	97	-0.8	1.6
15.1	e,rex,p	377	86	0.229	0.206	1.898 ± 0.025	0.1964 ± 0.0009	2796 ± 7	97		
16.1	e,osc/rex,p	67	35	0.524	0.110	1.355 ± 0.026	0.3491 ± 0.0045	3703 ± 20	95	-0.1	0.8
17.1	e,osc,p	253	162	0.640	0.054	1.352 ± 0.019	0.3560 ± 0.0022	3733 ± 9	94		
18.1	m,hb,p	60	50	0.839	0.054	1.299 ± 0.049	0.3463 ± 0.0139	3691 ± 61	100	-0.7	0.8
19.1	e,hd,p	1267	128	0.101	0.039	1.926 ± 0.037	0.1882 ± 0.0004	2726 ± 4	99	-4.7	1.0
20.1	r,hd,p	1367	21	0.015	0.034	1.976 ± 0.024	0.1846 ± 0.0005	2694 ± 4	98	-19.9	1.1
21.1	e,osc,p	240	34	0.142	0.158	1.801 ± 0.026	0.2062 ± 0.0012	2876 ± 9	99		
22.1	e,osc,p	572	456	0.797	0.150	2.062 ± 0.027	0.1920 ± 0.0008	2759 ± 7	91		
23.1	e,osc,p	229	129	0.564	0.079	1.748 ± 0.026	0.2119 ± 0.0012	2920 ± 9	100	4.6	1.1
24.1	m,osc,p	152	132	0.866	0.144	1.786 ± 0.029	0.2088 ± 0.0015	2896 ± 12	99		
25.1	e,h,p	239	87	0.363	0.038	1.815 ± 0.026	0.1958 ± 0.0021	2792 ± 17	102		
26.1	c,hd/rex,p	1869	1091	0.584	0.020	1.781 ± 0.021	0.1978 ± 0.0004	2808 ± 3	103	-0.3	1.0
27.1	e,osc,p	100	56	0.557	0.311	1.852 ± 0.033	0.1929 ± 0.0019	2767 ± 16	101	-1.2	1.0
28.1	m,osc,p	97	35	0.362	0.206	1.756 ± 0.031	0.2002 ± 0.0018	2828 ± 15	103		
29.1	e,hd,p	1327	277	0.209	0.050	2.251 ± 0.027	0.1664 ± 0.0005	2522 ± 5	93		

30.1	e,hd/rex,p	637	49	0.077	0.025	1.389 ± 0.018	0.3339 ± 0.0008	3635 ± 4	95		
31.1	e,hd,p	911	211	0.232	0.022	1.388 ± 0.017	0.3115 ± 0.0007	3528 ± 4	99		
32.1	e,osc,p,fr	67	24	0.352	0.183	1.270 ± 0.026	0.3893 ± 0.0027	3868 ± 10	96	-0.7	0.9
32.2	e,rex,p,fr	230	27	0.119	1.360	1.311 ± 0.018	0.3466 ± 0.0022	3692 ± 10	99		
32.3	e,rex,p,fr	119	26	0.223	0.110	1.270 ± 0.019	0.3550 ± 0.0011	3729 ± 5	101		
33.1	r,hd,p	283	99	0.349	0.087	2.040 ± 0.029	0.1898 ± 0.0011	2741 ± 10	93		
34.1	e,h/rex,p,fr	127	69	0.544	0.194	1.905 ± 0.032	0.1983 ± 0.0018	2812 ± 14	96		
35.1	r,h,p	235	33	0.142	0.127	1.935 ± 0.028	0.1975 ± 0.0012	2806 ± 10	95		
36.1	e,hd,p	1853	953	0.514	0.076	2.215 ± 0.027	0.1562 ± 0.0003	2414 ± 4	99	-14.2	1.4
37.1	e,h,p,fr	337	154	0.456	0.077	1.956 ± 0.027	0.1874 ± 0.0010	2720 ± 9	97	-6.2	0.8
38.1	e,osc,p	221	49	0.222	0.139	1.880 ± 0.028	0.1979 ± 0.0014	2809 ± 12	97	1.3	0.9
39.1	e,osc/rex,p,fr	63	34	0.540	0.655	1.840 ± 0.040	0.1905 ± 0.0030	2746 ± 25	102	-0.5	0.7
40.1	m,h,p	136	91	0.665	0.012	1.861 ± 0.026	0.2048 ± 0.0011	2865 ± 9	96		
41.1	m,osc,p	580	214	0.370	0.211	1.921 ± 0.023	0.1912 ± 0.0006	2752 ± 5	98	-2.8	1.7
42.1	e,hd,p	159	33	0.206	0.091	1.438 ± 0.028	0.3110 ± 0.0012	3526 ± 6	95		
43.1	e,osc,p	547	93	0.169	0.053	1.819 ± 0.025	0.1975 ± 0.0005	2806 ± 4	101		
44.1	e,osc,p	53	29	0.548	0.529	1.853 ± 0.033	0.1884 ± 0.0020	2728 ± 18	102	-2.2	0.9
45.1	e,hd,p	420	29	0.069	0.072	1.813 ± 0.023	0.2028 ± 0.0006	2849 ± 5	99		
46.1	e,osc/h,p	319	46	0.145	0.000	2.051 ± 0.031	0.1937 ± 0.0007	2774 ± 6	91		
47.1	m,osc,eq	75	111	1.493	0.045	1.819 ± 0.030	0.1974 ± 0.0015	2804 ± 12	101		
48.1	e,hd,h	1082	33	0.030	bld	1.868 ± 0.022	0.1971 ± 0.0004	2803 ± 3	98	-1.1	0.8
49.1	e,osc,p	488	115	0.236	0.237	1.985 ± 0.024	0.1952 ± 0.0006	2787 ± 5	93		
50.1	e,osc,p	144	41	0.281	0.035	1.813 ± 0.026	0.2009 ± 0.0011	2833 ± 9	100	1.6	1.0
51.1	e,h,eq	398	3	0.009	0.009	1.948 ± 0.024	0.1824 ± 0.0006	2675 ± 6	100	-22.6	0.7
52.1	e,osc,p	220	55	0.252	0.071	1.830 ± 0.024	0.1994 ± 0.0009	2822 ± 7	100		
53.1	e,osc/h,eq	142	45	0.319	0.059	1.856 ± 0.027	0.1992 ± 0.0011	2819 ± 9	98	1.0	0.8
54.1	e,osc,p	221	256	1.157	0.116	1.701 ± 0.023	0.2280 ± 0.0009	3038 ± 7	98		
55.1	e,h,p	189	108	0.574	0.072	1.852 ± 0.025	0.1956 ± 0.0009	2790 ± 8	100	0.1	1.5
56.1	e,osc,p	105	61	0.581	0.239	1.399 ± 0.021	0.3340 ± 0.0035	3636 ± 16	94		
57.1	e,h,p,fr	420	325	0.773	0.000	1.887 ± 0.024	0.1950 ± 0.0006	2785 ± 5	98		
58.1	e,osc,p	673	414	0.614	0.096	1.868 ± 0.023	0.2023 ± 0.0005	2845 ± 4	96	1.7	1.1
59.1	e,osc,p	151	42	0.278	0.085	1.987 ± 0.028	0.1995 ± 0.0010	2822 ± 9	92		
60.1	e,h,p	340	18	0.052	0.016	1.291 ± 0.017	0.3434 ± 0.0014	3678 ± 6	101	-0.7	0.9
61.1	e,hd,p	3433	106	0.031	0.004	1.999 ± 0.023	0.1768 ± 0.0002	2623 ± 2	100	-22.9	0.9
62.1	e,osc,p	275	26	0.095	0.018	1.277 ± 0.017	0.3847 ± 0.0010	3850 ± 4	96	-0.3	1.0
63.1	e,osc,p	114	71	0.620	0.045	1.763 ± 0.026	0.2109 ± 0.0013	2912 ± 10	99	2.2	0.9
64.1	e,hd,p	381	110	0.287	0.010	1.911 ± 0.024	0.1886 ± 0.0007	2730 ± 6	99	-0.1	0.9
65.1	e,osc,p	203	111	0.548	0.220	1.969 ± 0.026	0.2034 ± 0.0010	2854 ± 8	91		
66.1	e,h,p	452	46	0.102	0.025	1.458 ± 0.018	0.3133 ± 0.0007	3537 ± 4	94		

67.1	e,osc/h,p	378	267	0.705	0.030	1.468 ± 0.018	0.2951 ± 0.0019	3445 ± 10	96		
68.1	e,osc,p	87	33	0.384	0.074	1.754 ± 0.028	0.2100 ± 0.0014	2905 ± 11	100	2.7	0.8
69.1	e,osc,p	115	44	0.382	0.055	1.782 ± 0.027	0.1973 ± 0.0013	2804 ± 10	103	0.6	0.8
70.1	e,osc,p,fr	168	132	0.785	0.097	1.841 ± 0.026	0.1988 ± 0.0011	2816 ± 9	99	1.0	0.8
71.1	m,hd,p	880	15	0.018	0.020	2.286 ± 0.030	0.1625 ± 0.0005	2482 ± 5	93		
72.1	m,h,p	391	327	0.835	0.022	1.742 ± 0.024	0.2163 ± 0.0004	2953 ± 3	99	0.1	1.4
73.1	e,h,p	301	310	1.029	0.017	1.339 ± 0.019	0.3329 ± 0.0011	3631 ± 5	99	-0.8	1.3
74.1	m,osc/h,p	272	166	0.611	0.037	1.760 ± 0.024	0.2002 ± 0.0005	2828 ± 4	103	2.7	1.3
75.1	e,osc,p	265	17	0.063	0.020	1.794 ± 0.025	0.2000 ± 0.0006	2827 ± 5	101	0.3	0.7
sand #4 (eastern Ujaragssuit nunaat: 64°58.75'N 49°56.28'W - WGS84 datum)											
1.1	e,osc,p	257	136	0.527	0.379	2.006 ± 0.026	0.2035 ± 0.0010	2855 ± 8	89		
2.1	e,osc,p	197	140	0.712	0.021	1.279 ± 0.017	0.3330 ± 0.0011	3631 ± 5	103		
3.1	e,osc,p	265	38	0.145	0.102	1.333 ± 0.017	0.3771 ± 0.0024	3820 ± 10	93		
4.1	m,h,p	465	226	0.486	0.029	1.320 ± 0.016	0.3630 ± 0.0007	3763 ± 3	96	-23.9	1.1
5.1	e,h,p	388	7	0.018	0.018	1.921 ± 0.024	0.1853 ± 0.0006	2701 ± 6	100		
6.1	e,hd/rex,p	1967	2074	1.054	0.101	2.626 ± 0.031	0.1621 ± 0.0003	2478 ± 3	81		
7.1	e,h,p,fr	349	139	0.399	0.186	1.840 ± 0.024	0.2164 ± 0.0008	2954 ± 6	93		
8.1	e,h,p	2239	661	0.295	0.031	1.784 ± 0.021	0.2029 ± 0.0005	2849 ± 4	101	0.4	0.8
9.1	e,hd,p	547	1	0.002	0.003	1.624 ± 0.020	0.2288 ± 0.0006	3044 ± 4	102	-12.5	0.9
10.1	e,h,eq	392	55	0.140	0.048	1.320 ± 0.017	0.3375 ± 0.0013	3651 ± 6	99	1.1	1.0
11.1	e,h,p	518	107	0.207	0.008	1.319 ± 0.016	0.3354 ± 0.0006	3642 ± 3	100	-2.5	0.7
12.1	e,osc,p	712	212	0.298	0.238	2.744 ± 0.121	0.3302 ± 0.0010	3618 ± 5	48		
13.1	m,h,p	1699	64	0.038	0.004	1.269 ± 0.015	0.3374 ± 0.0004	3651 ± 2	103		
14.1	e,osc,p	294	39	0.131	0.110	1.338 ± 0.017	0.3452 ± 0.0009	3686 ± 4	97	-5.9	0.8
14.1	duplicate Hf									-8.5	0.9
15.1	e,osc,p	121	64	0.531	0.188	1.302 ± 0.019	0.3649 ± 0.0025	3770 ± 11	97		
16.1	e,osc,p	227	69	0.305	0.076	1.305 ± 0.017	0.3489 ± 0.0018	3702 ± 8	99	-2.2	0.8
17.1	e,hd,p	1892	443	0.234	0.117	1.348 ± 0.016	0.3434 ± 0.0004	3678 ± 2	96		
18.1	e,osc,p	106	42	0.393	0.028	1.210 ± 0.018	0.3848 ± 0.0015	3851 ± 6	101	1.5	1.1
19.1	e,osc/h,p	91	42	0.461	0.044	1.232 ± 0.019	0.3725 ± 0.0016	3802 ± 7	101	-0.5	0.8
19.1	duplicate Hf									0.1	0.7
20.1	e,hd/rex,p	1732	32	0.018	0.078	1.631 ± 0.019	0.2396 ± 0.0009	3117 ± 6	99	-11.3	1.6
21.1	m,osc,eq	233	122	0.525	0.062	1.246 ± 0.017	0.3729 ± 0.0010	3803 ± 4	100		
22.1	e,h,p	333	89	0.268	0.019	1.673 ± 0.021	0.2178 ± 0.0020	2965 ± 15	102		
23.1	e,osc/rex,p	206	110	0.530	0.081	1.249 ± 0.017	0.3794 ± 0.0011	3829 ± 4	99	0.2	0.9
24.1	e,osc,p,fr	224	39	0.175	0.066	1.812 ± 0.024	0.1971 ± 0.0009	2802 ± 8	101	0.5	0.9
24.1	duplicate Hf									-1.9	1.0
25.1	e,h/rex,p	772	29	0.038	0.070	1.436 ± 0.017	0.3075 ± 0.0023	3508 ± 12	96		

26.1	r,h,p	172	83	0.480	0.102	1.315 ± 0.018	0.3405 ± 0.0012	3665 ± 5	99		
27.1	e,osc/h,p	1147	331	0.288	0.041	1.220 ± 0.015	0.3845 ± 0.0012	3849 ± 5	100		
28.1	e,hd,p	2462	74	0.030	0.005	1.344 ± 0.016	0.3250 ± 0.0012	3594 ± 6	100	-3.4	1.2
29.1	e,osc,p	113	53	0.472	0.029	1.667 ± 0.025	0.2194 ± 0.0022	2976 ± 16	102		
30.1	e,hd,p,fr	654	125	0.192	0.012	1.348 ± 0.016	0.3298 ± 0.0006	3616 ± 3	99		
31.1	e,osc,p,fr	446	440	0.986	0.163	1.849 ± 0.031	0.2038 ± 0.0007	2857 ± 5	97		
32.1	e,osc,p	231	54	0.234	0.086	1.879 ± 0.025	0.1958 ± 0.0009	2792 ± 7	98	-0.4	0.8
33.1	e,osc,p	365	125	0.341	0.096	1.810 ± 0.023	0.1962 ± 0.0007	2795 ± 6	102	-0.3	0.6
34.1	m,osc,eq	200	147	0.735	0.028	1.266 ± 0.017	0.3869 ± 0.0011	3859 ± 4	96	0.1	0.9
35.1	e,hd,p	1000	73	0.073	0.077	1.386 ± 0.017	0.3242 ± 0.0005	3590 ± 2	97	-2.9	1.0
36.1	e,osc,p	372	69	0.184	0.879	1.320 ± 0.017	0.3526 ± 0.0015	3718 ± 6	97		
37.1	m,osc,p	276	146	0.530	0.202	1.931 ± 0.025	0.2023 ± 0.0008	2845 ± 7	93		
38.1	e,h,p	1921	138	0.072	0.660	1.808 ± 0.021	0.2012 ± 0.0007	2836 ± 6	100		
39.1	e,osc,p,fr	471	70	0.148	0.028	1.353 ± 0.017	0.3585 ± 0.0008	3744 ± 3	94		
40.1	e,hd,p	989	891	0.901	0.077	1.363 ± 0.016	0.3196 ± 0.0005	3568 ± 2	99		
41.1	e,osc,p	199	125	0.628	0.049	1.231 ± 0.017	0.3866 ± 0.0011	3858 ± 4	99	0.0	1.1
42.1	e,h/rex,p	188	60	0.320	0.121	1.508 ± 0.021	0.2643 ± 0.0010	3273 ± 6	100	-7.6	1.1
43.1	e,osc,p,fr	247	35	0.143	0.014	1.811 ± 0.024	0.2024 ± 0.0008	2846 ± 7	100	0.9	0.8
44.1	e,hd,eq	241	75	0.311	0.037	1.298 ± 0.017	0.3359 ± 0.0011	3644 ± 5	101	-0.7	0.8
45.1	e,osc,p	132	105	0.794	0.075	1.229 ± 0.018	0.3838 ± 0.0024	3847 ± 10	100	-0.4	0.9
46.1	e,hd,p	2678	86	0.032	0.254	2.474 ± 0.029	0.1498 ± 0.0003	2343 ± 3	92		
47.1	e,h,p	378	48	0.127	0.030	1.285 ± 0.016	0.3465 ± 0.0008	3692 ± 3	101	1.9	1.0
48.1	e,hd,p	415	221	0.532	0.032	1.915 ± 0.024	0.1873 ± 0.0006	2718 ± 6	100	-10.6	0.7
49.1	e,h,p	607	634	1.044	0.011	1.773 ± 0.022	0.2050 ± 0.0005	2867 ± 4	101	0.3	1.4
50.1	e,osc,p,fr	88	27	0.311	bld	1.211 ± 0.019	0.3797 ± 0.0017	3831 ± 7	102	0.5	0.8
51.1	r,h,p	1403	79	0.057	0.042	2.067 ± 0.024	0.1725 ± 0.0003	2582 ± 3	98	-4.2	0.9
52.1	m,osc,eq	508	65	0.128	0.017	1.615 ± 0.026	0.2841 ± 0.0006	3386 ± 3	90		
53.1	e,osc,p	164	108	0.655	0.020	1.796 ± 0.025	0.2061 ± 0.0010	2875 ± 8	99		
54.1	r,h,p	2362	137	0.058	0.006	1.753 ± 0.021	0.2172 ± 0.0003	2960 ± 2	98	-19.3	1.0
55.1	e,hd,p	909	129	0.142	2.539	2.191 ± 0.026	0.1865 ± 0.0009	2712 ± 8	87		
57.1	e,h,p	117	102	0.869	0.084	1.782 ± 0.026	0.2053 ± 0.0012	2869 ± 10	100		
58.1	e,hd,p	970	130	0.134	0.396	1.559 ± 0.019	0.3276 ± 0.0015	3606 ± 7	86		
59.1	e,h,p	240	57	0.236	0.051	1.817 ± 0.024	0.1979 ± 0.0008	2809 ± 7	101		
60.1	e,osc/h,p,fr	191	28	0.149	0.068	1.772 ± 0.024	0.2011 ± 0.0009	2835 ± 8	102		
61.1	e,h,p,fr	1332	984	0.738	0.026	1.352 ± 0.016	0.3266 ± 0.0004	3601 ± 2	99	-3.7	1.2
62.1	e,h,p	937	342	0.364	0.183	1.925 ± 0.023	0.1976 ± 0.0004	2806 ± 4	95		
63.1	e,hd,p	1099	44	0.040	0.010	1.386 ± 0.017	0.3291 ± 0.0011	3613 ± 5	96	-4.4	1.5
64.1	e,osc,p	419	302	0.721	0.036	1.241 ± 0.015	0.3844 ± 0.0008	3849 ± 3	99		
65.1	e,osc,p,fr	83	40	0.488	0.054	1.684 ± 0.027	0.2187 ± 0.0023	2971 ± 17	101		

66.1	e,h,p	66	34	0.517	bld	1.294 ± 0.022	0.3347 ± 0.0018	3639 ± 8	102	0.1	0.9
67.1	e,osc,p	260	150	0.577	0.155	1.804 ± 0.023	0.2037 ± 0.0008	2856 ± 7	99	1.9	0.8
68.1	e,hd,p	533	246	0.461	0.043	1.979 ± 0.024	0.1934 ± 0.0005	2772 ± 5	94		
69.1	e,osc,p	250	123	0.493	0.032	1.221 ± 0.016	0.3867 ± 0.0020	3858 ± 8	100		
70.1	e,osc,p	214	102	0.477	0.044	1.795 ± 0.024	0.2044 ± 0.0009	2862 ± 7	100	2.0	1.0
71.1	e,h,p	224	110	0.489	0.180	1.816 ± 0.025	0.2038 ± 0.0006	2857 ± 5	99		
72.1	e,osc,p	108	47	0.436	0.045	1.310 ± 0.020	0.3341 ± 0.0012	3636 ± 5	101	2.9	2.6
73.1	e,h/rex,p	376	129	0.344	0.306	1.628 ± 0.022	0.3129 ± 0.0012	3535 ± 6	84		
74.1	e,rex,p	32	1	0.026	0.024	1.246 ± 0.023	0.3461 ± 0.0018	3690 ± 8	104		
75.1	m,osc,p	264	166	0.630	0.051	1.852 ± 0.026	0.2032 ± 0.0005	2852 ± 4	97		
76.1	e,osc,p	147	63	0.426	0.009	1.843 ± 0.027	0.2047 ± 0.0007	2864 ± 6	97		
77.1	m,h,p	262	58	0.222	0.107	1.295 ± 0.018	0.3734 ± 0.0007	3805 ± 3	96	0.1	1.0

Rock samples

G03/18 gneiss totally retrogressed from granulite facies with mafic dyke remnants, Ameralla

Neosome

2.1	e,osc,p	299	80	0.267	0.001	1.353 ± 0.039	0.3309 ± 0.0014	3621 ± 7	99
3.1	e,osc,p	1181	120	0.102	0.070	1.774 ± 0.032	0.1988 ± 0.0013	2817 ± 10	102
6.1	m,osc,p,fr	318	91	0.287	0.045	1.371 ± 0.051	0.3179 ± 0.0009	3560 ± 5	99
7.1	m,osc,p	250	153	0.614	0.265	1.846 ± 0.057	0.1985 ± 0.0010	2813 ± 9	99
4.1	e,osc,p	968	66	0.068	0.014	1.794 ± 0.066	0.2037 ± 0.0009	2856 ± 7	100
5.1	e,osc,p	608	188	0.310	0.195	1.750 ± 0.054	0.2023 ± 0.0008	2845 ± 7	102
8.1	e,osc/h,p	1288	460	0.357	0.099	1.769 ± 0.051	0.2056 ± 0.0006	2871 ± 4	101
9.1	m,osc,p,fr	335	74	0.221	0.018	1.785 ± 0.044	0.2040 ± 0.0011	2858 ± 9	100
10.1	e,osc,p	403	79	0.196	0.010	1.340 ± 0.023	0.3248 ± 0.0013	3593 ± 6	100
11.1	m/c,osc,p	405	58	0.142	0.097	1.575 ± 0.049	0.2636 ± 0.0011	3268 ± 7	97
12.1	m/c,osc,p	268	48	0.181	0.160	1.772 ± 0.056	0.2031 ± 0.0016	2852 ± 13	101

Palaeosome

1.1	c,osc,p	55	50	0.907	0.043	1.333 ± 0.037	0.3251 ± 0.0029	3594 ± 14	100
2.1	e,hd,p	705	23	0.032	0.007	1.864 ± 0.022	0.1960 ± 0.0007	2793 ± 6	99
3.1	c,h,p	63	89	1.413	0.021	1.290 ± 0.028	0.3305 ± 0.0020	3619 ± 9	102
4.1	r,hd/osc,p	1356	22	0.016	0.024	1.937 ± 0.039	0.1963 ± 0.0005	2795 ± 4	96
5.1	e,osc,p	75	36	0.473	0.001	1.210 ± 0.024	0.3804 ± 0.0049	3833 ± 19	101
6.1	c,h/osc,p	56	79	1.409	0.001	1.331 ± 0.033	0.3222 ± 0.0027	3580 ± 13	101

437605 gneiss totally retrogressed from granulite facies with mafic dyke remnants, Ameralla

1.1	c,osc,p,fr	214	315	1.469	0.020	1.806 ± 0.080	0.2058 ± 0.0024	2873 ± 19	99
1.2	r,h,p,fr	268	11	0.041	0.021	1.757 ± 0.083	0.1939 ± 0.0007	2775 ± 6	105
2.1	c,osc,p,fr	117	122	1.046	0.009	1.798 ± 0.100	0.2087 ± 0.0018	2896 ± 14	98

2.2	r,h,p,fr	129	54	0.415	0.009	1.722	±	0.094	0.2049	±	0.0008	2866 ± 6	103
3.1	r,h,p	354	19	0.054	0.005	1.824	±	0.099	0.1932	±	0.0009	2769 ± 7	102
4.1	m,osc,p,fr	123	115	0.931	0.022	1.895	±	0.115	0.2020	±	0.0023	2843 ± 19	96
5.1	r,h,p	321	17	0.052	0.005	1.710	±	0.096	0.1895	±	0.0026	2737 ± 22	108

all uncertainties in the Table are given at 1 sigma.
Site: x.y, x=grain number, y=analysis number.
Grain and site character: p=prism, eq=small aspect ratio prism, fr=grain fragment, t=turbid
e=end analysis site, m=middle analysis site, r=rim, c=core
CL imagery: osc=oscillatory finescale zoning, h=homogeneous, hb=bright and homogeneous, hd=non-luminescent, rex=recrystallised,
Common Pb correction: comm 206%= percentage of Pb that is non-radiogenic, based on measured ^{204}Pb
and common Pb = likely age of grain based on the model of Cumming and Richards (1975)
bld = ^{204}Pb not detected.
εHf (t-zircon) -see Table 2 for complete Lu-Hf data

Table 2

grain[a]	$^{174}Hf/^{177}Hf$	1SE in run errors	$^{178}Hf/^{177}Hf$	1SE	$^{176}Lu/^{177}Hf$	1SE	Measured $^{176}Hf/^{177}Hf$	1SE	present day epsilon Hf εHf(0)	1SE	U/Pb AGE	1SE
Sand #1												
4	0.008587	0.000017	1.467260	0.000062	0.000870	0.000046	0.280302	0.000018	-87.79	0.63	3783	3
5	0.008683	0.000017	1.467476	0.000087	0.000471	0.000013	0.280467	0.000012	-81.97	0.42	3642	3
6	0.008671	0.000006	1.467339	0.000028	0.000417	0.000016	0.280298	0.000008	-87.96	0.29	3595	6
7a[b]	0.008670	0.000011	1.467311	0.000100	0.000500	0.000004	0.280383	0.000024	-84.92	0.84	3696	5
7b[b]	0.008636	0.000015	1.467396	0.000111	0.000384	0.000008	0.280277	0.000024	-88.68	0.86	3898	6
8	0.008646	0.000019	1.467357	0.000054	0.000548	0.000034	0.280436	0.000014	-83.05	0.49	3610	5
9	0.008667	0.000015	1.467302	0.000071	0.000381	0.000014	0.280345	0.000015	-86.30	0.54	3786	10
12	0.008569	0.000016	1.467384	0.000052	0.001151	0.000055	0.280475	0.000011	-81.68	0.40	3648	2
14	0.008640	0.000012	1.467359	0.000035	0.001170	0.000034	0.280456	0.000009	-82.37	0.31	3656	6
16	0.008603	0.000020	1.467478	0.000143	0.000269	0.000034	0.280310	0.000026	-87.53	0.92	3771	2
22	0.008654	0.000006	1.467350	0.000032	0.000364	0.000003	0.280396	0.000008	-84.48	0.29	3613	5
27	0.008666	0.000009	1.467410	0.000050	0.000161	0.000004	0.280342	0.000011	-86.38	0.41	3619	6
32	0.008663	0.000013	1.467348	0.000029	0.001212	0.000028	0.280359	0.000010	-85.81	0.37	3846	6
39	0.008655	0.000011	1.467320	0.000036	0.000726	0.000023	0.280382	0.000009	-84.98	0.34	3809	5
57	0.008655	0.000019	1.467356	0.000079	0.000629	0.000032	0.280990	0.000018	-63.48	0.62	2951	6
60a	0.008656	0.000008	1.467387	0.000039	0.000344	0.000016	0.280314	0.000008	-87.37	0.30	3888	9
60b	0.008651	0.000010	1.467359	0.000038	0.000695	0.000021	0.280326	0.000010	-86.96	0.35	3888	9
62	0.008626	0.000008	1.467370	0.000038	0.000925	0.000027	0.280516	0.000007	-80.23	0.26	3631	4
66	0.008655	0.000013	1.467299	0.000043	0.000543	0.000028	0.280389	0.000011	-84.73	0.40	3667	14
68	0.008614	0.000027	1.467295	0.000034	0.001333	0.000059	0.280425	0.000014	-83.47	0.49	3711	4
72	0.008639	0.000011	1.467367	0.000038	0.000452	0.000030	0.280318	0.000012	-87.24	0.41	3803	10
Sand #2												
5	0.008648	0.000011	1.467360	0.000038	0.001054	0.000013	0.280419	0.000009	-83.68	0.33	3716	4
6	0.008655	0.000007	1.467371	0.000030	0.000651	0.000012	0.280436	0.000007	-83.08	0.25	3619	2
7	0.008660	0.000020	1.467365	0.000043	0.000583	0.000028	0.280728	0.000017	-72.75	0.60	2729	2

8	0.008658	0.000014	1.467402	0.000052	0.000803	0.000014	0.280376	0.000013	-85.19	0.45	3794	4
14	0.008660	0.000012	1.467306	0.000042	0.000688	0.000033	0.280414	0.000013	-83.83	0.45	3702	5
17	0.008627	0.000011	1.467356	0.000046	0.000716	0.000018	0.280749	0.000012	-72.01	0.42	2871	4
19	0.008639	0.000008	1.467402	0.000061	0.000648	0.000007	0.281005	0.000011	-62.94	0.40	2713	3
20	0.008649	0.000012	1.467445	0.000053	0.000717	0.000036	0.280487	0.000013	-81.27	0.46	2696	3
21	0.008667	0.000011	1.467338	0.000029	0.000821	0.000023	0.281028	0.000009	-62.12	0.33	2858	6
22	0.008644	0.000009	1.467339	0.000031	0.000816	0.000020	0.280454	0.000009	-82.42	0.30	3594	4
25	0.008667	0.000010	1.467337	0.000063	0.000649	0.000031	0.281002	0.000018	-63.05	0.65	2834	7
27	0.008643	0.000015	1.467328	0.000057	0.000795	0.000028	0.280421	0.000012	-83.60	0.41	3640	1
30	0.008669	0.000010	1.467357	0.000041	0.000397	0.000010	0.280310	0.000011	-87.52	0.40	3892	7
32	0.008645	0.000011	1.467332	0.000041	0.000658	0.000015	0.280318	0.000010	-87.25	0.36	3848	13
38	0.008679	0.000011	1.467275	0.000032	0.001386	0.000026	0.280456	0.000008	-82.35	0.29	3677	5
39	0.008656	0.000010	1.467368	0.000031	0.000470	0.000006	0.280502	0.000009	-80.73	0.33	3631	12
40	0.008637	0.000012	1.467288	0.000036	0.001271	0.000042	0.280437	0.000012	-83.05	0.41	3679	3
44	0.008658	0.000008	1.467378	0.000041	0.000470	0.000007	0.281018	0.000011	-62.49	0.40	2897	10
45	0.008650	0.000009	1.467345	0.000031	0.000548	0.000015	0.280418	0.000009	-83.69	0.32	3623	5
47	0.008664	0.000007	1.467362	0.000028	0.000713	0.000004	0.280711	0.000007	-73.33	0.23	2709	6
48	0.008659	0.000007	1.467353	0.000030	0.000889	0.000013	0.280375	0.000009	-85.23	0.32	3736	3
51	0.008683	0.000019	1.467373	0.000062	0.000622	0.000017	0.280683	0.000012	-74.34	0.42	2630	2
53	0.008654	0.000008	1.467346	0.000037	0.000495	0.000007	0.280471	0.000010	-81.83	0.37	3575	2
56	0.008665	0.000021	1.467523	0.000065	0.000178	0.000029	0.280715	0.000017	-73.18	0.60	2727	7
57	0.008628	0.000014	1.467349	0.000042	0.001081	0.000025	0.281048	0.000012	-61.41	0.44	2766	5
61	0.008663	0.000014	1.467311	0.000049	0.000534	0.000026	0.280423	0.000013	-83.52	0.46	3686	4
66	0.008615	0.000018	1.467319	0.000050	0.000673	0.000053	0.280442	0.000014	-82.84	0.48	3647	4
67a	0.008493	0.000050	1.467330	0.000073	0.002838	0.000228	0.280550	0.000026	-79.04	0.92	3775	2
67b	0.008500	0.000049	1.467343	0.000072	0.002859	0.000220	0.280553	0.000025	-78.92	0.90	3775	2
71	0.008625	0.000019	1.467350	0.000036	0.001051	0.000028	0.280595	0.000011	-77.43	0.37	2719	2
73	0.008558	0.000012	1.467403	0.000043	0.001092	0.000093	0.280820	0.000012	-69.48	0.44	2580	2
75	0.008675	0.000023	1.467329	0.000050	0.000970	0.000053	0.280377	0.000014	-85.14	0.48	3725	4
Sand #3												
2	0.008594	0.000015	1.467437	0.000078	0.000899	0.000043	0.281004	0.000015	-63.00	0.52	2952	5
4	0.008635	0.000018	1.467266	0.000056	0.001268	0.000033	0.280446	0.000012	-82.71	0.41	3706	4

5	0.008656	0.000014	1.467421	0.000087	0.000347	0.000004	0.281047	0.000014	-61.46	0.51	2788	19
7	0.008661	0.000012	1.467333	0.000055	0.000154	0.000004	0.280936	0.000014	-65.40	0.50	2817	6
12	0.008634	0.000018	1.467629	0.000119	0.000798	0.000007	0.281094	0.000019	-59.80	0.68	2880	10
14	0.008661	0.000013	1.467565	0.000098	0.000484	0.000025	0.281021	0.000023	-62.39	0.80	2748	5
16	0.008659	0.000009	1.467339	0.000033	0.000626	0.000034	0.280426	0.000010	-83.43	0.35	3703	20
18	0.008653	0.000008	1.467376	0.000050	0.000206	0.000003	0.280384	0.000010	-84.89	0.35	3691	61
19	0.008652	0.000016	1.467352	0.000061	0.001419	0.000025	0.280975	0.000012	-64.02	0.43	2726	4
20	0.008670	0.000007	1.467537	0.000075	0.000188	0.000006	0.280505	0.000015	-80.64	0.52	2694	4
23	0.008640	0.000013	1.467549	0.000089	0.000618	0.000007	0.281069	0.000014	-60.67	0.51	2920	9
26	0.008554	0.000018	1.467422	0.000045	0.001549	0.000083	0.281053	0.000013	-61.25	0.44	2808	3
27	0.008656	0.000014	1.467369	0.000038	0.000797	0.000021	0.281015	0.000012	-62.59	0.44	2767	17
32	0.008577	0.000020	1.467309	0.000049	0.000687	0.000059	0.280303	0.000011	-87.78	0.39	3868	10
36	0.008684	0.000009	1.467648	0.000082	0.000393	0.000012	0.280856	0.000019	-68.21	0.66	2414	4
37	0.008630	0.000010	1.467374	0.000034	0.000838	0.000028	0.280907	0.000010	-66.40	0.36	2720	9
38	0.008655	0.000007	1.467458	0.000050	0.000221	0.000006	0.281026	0.000011	-62.20	0.40	2809	9
39	0.008667	0.000006	1.467339	0.000036	0.000476	0.000010	0.281030	0.000008	-62.07	0.29	2746	25
41	0.008614	0.000018	1.467224	0.000046	0.001078	0.000056	0.280995	0.000023	-63.30	0.83	2752	5
44	0.008666	0.000011	1.467389	0.000038	0.000672	0.000009	0.281006	0.000011	-62.92	0.37	2728	18
48	0.008643	0.000008	1.467361	0.000044	0.000520	0.000008	0.280979	0.000010	-63.87	0.36	2803	3
50	0.008657	0.000010	1.467400	0.000056	0.000260	0.000002	0.281021	0.000015	-62.39	0.51	2833	9
51	0.008669	0.000007	1.467344	0.000031	0.000030	0.000001	0.280432	0.000008	-83.21	0.28	2675	6
53	0.008666	0.000010	1.467353	0.000031	0.000390	0.000007	0.281020	0.000009	-62.42	0.34	2819	9
55	0.008666	0.000034	1.467302	0.000058	0.000950	0.000055	0.281045	0.000020	-61.53	0.69	2790	8
58	0.008653	0.000024	1.467308	0.000070	0.001950	0.000021	0.281109	0.000015	-59.27	0.53	2845	4
60	0.008561	0.000022	1.467354	0.000035	0.002554	0.000046	0.280562	0.000011	-78.61	0.39	3678	6
61	0.008632	0.000015	1.467476	0.000044	0.000827	0.000035	0.280500	0.000011	-80.82	0.40	2623	2
62	0.008647	0.000012	1.467362	0.000048	0.000534	0.000039	0.280314	0.000012	-87.37	0.43	3850	4
63	0.008665	0.000012	1.467306	0.000036	0.000968	0.000024	0.281024	0.000011	-62.26	0.38	2912	10
64	0.008646	0.000010	1.467442	0.000041	0.000561	0.000018	0.281057	0.000011	-61.12	0.38	2730	6
68	0.008654	0.000010	1.467393	0.000044	0.000948	0.000007	0.281042	0.000010	-61.64	0.35	2905	11
69	0.008665	0.000009	1.467344	0.000031	0.000683	0.000012	0.281036	0.000009	-61.86	0.32	2804	10
70	0.008663	0.000010	1.467307	0.000035	0.000733	0.000032	0.281041	0.000010	-61.68	0.35	2816	9
72	0.008544	0.000072	1.467436	0.000110	0.002262	0.000074	0.281015	0.000019	-62.61	0.69	2953	5

73	0.008630	0.000012	1.467384	0.000061	0.000593	0.000005	0.280450	0.000018	-82.57	0.63	3631	5
74	0.008634	0.000012	1.467586	0.000071	0.000460	0.000027	0.281066	0.000017	-60.79	0.60	2828	4
75	0.008655	0.000008	1.467355	0.000037	0.000522	0.000008	0.281004	0.000009	-62.99	0.31	2827	5
Sand #4												
5	0.008646	0.000011	1.467460	0.000060	0.000375	0.000008	0.280396	0.000014	-84.49	0.50	2701	6
8	0.008646	0.000011	1.467356	0.000036	0.001144	0.000031	0.281024	0.000010	-62.26	0.36	2849	4
9	0.008662	0.000005	1.467385	0.000037	0.000219	0.000004	0.280484	0.000010	-81.35	0.37	3044	4
10	0.008580	0.000023	1.467421	0.000061	0.002313	0.000048	0.280612	0.000013	-76.84	0.46	3651	6
11	0.008650	0.000009	1.467402	0.000037	0.000328	0.000003	0.280377	0.000009	-85.15	0.31	3642	3
14	0.008669	0.000009	1.467364	0.000035	0.000681	0.000015	0.280277	0.000010	-88.69	0.37	3686	4
14b	0.008641	0.000011	1.467274	0.000039	0.000708	0.000028	0.280205	0.000011	-91.24	0.41	3686	4
16	0.008677	0.000006	1.467368	0.000044	0.000299	0.000003	0.280344	0.000010	-86.33	0.37	3702	8
18	0.008655	0.000013	1.467437	0.000070	0.000374	0.000012	0.280354	0.000015	-85.98	0.53	3851	6
19	0.008665	0.000007	1.467354	0.000031	0.000270	0.000001	0.280321	0.000009	-87.12	0.33	3802	7
19b	0.008651	0.000010	1.467339	0.000029	0.000555	0.000008	0.280359	0.000008	-85.80	0.28	3802	7
20	0.008669	0.000006	1.467610	0.000095	0.000331	0.000004	0.280476	0.000022	-81.66	0.78	3117	6
23	0.008665	0.000010	1.467391	0.000037	0.000571	0.000012	0.280344	0.000011	-86.31	0.39	3829	4
24	0.008648	0.000012	1.467397	0.000049	0.000608	0.000018	0.281029	0.000012	-62.11	0.41	2802	4
24b	0.008650	0.000013	1.467253	0.000063	0.000501	0.000021	0.280298	0.000014	-87.94	0.48	3803	10
28	0.008674	0.000013	1.467442	0.000041	0.001049	0.000030	0.280432	0.000015	-83.20	0.54	3594	6
32	0.008643	0.000015	1.467346	0.000035	0.001214	0.000042	0.281043	0.000010	-61.61	0.36	2792	7
33	0.008665	0.000008	1.467329	0.000036	0.000381	0.000010	0.280999	0.000007	-63.15	0.25	2795	6
34	0.008632	0.000012	1.467270	0.000037	0.000724	0.000024	0.280335	0.000011	-86.63	0.39	3859	4
35	0.008651	0.000008	1.467449	0.000062	0.000298	0.000005	0.280398	0.000013	-84.39	0.45	3590	2
41	0.008645	0.000014	1.467293	0.000062	0.000527	0.000016	0.280318	0.000014	-87.23	0.49	3858	4
42	0.008620	0.000022	1.467386	0.000081	0.001258	0.000026	0.280537	0.000015	-79.50	0.54	3273	6
43	0.008657	0.000008	1.467398	0.000038	0.000505	0.000007	0.281005	0.000010	-62.96	0.35	2846	7
44	0.008657	0.000006	1.467355	0.000033	0.000073	0.000003	0.280408	0.000009	-84.05	0.32	3644	5
45	0.008614	0.000011	1.467350	0.000058	0.000566	0.000016	0.280317	0.000012	-87.26	0.41	3847	10
47	0.008663	0.000010	1.467551	0.000062	0.000561	0.000004	0.280482	0.000013	-81.43	0.47	3692	10
48	0.008649	0.000009	1.467345	0.000035	0.000586	0.000005	0.280770	0.000009	-71.25	0.31	2718	10
49	0.008603	0.000036	1.467400	0.000045	0.002280	0.000134	0.281073	0.000019	-60.54	0.68	2867	10

50	0.008652	0.000008	1.467386	0.000042	0.000258	0.000002	0.280329	0.000010	-86.86	0.35	3831	7
51	0.008673	0.000011	1.467356	0.000042	0.000583	0.000040	0.281038	0.000011	-61.76	0.40	2582	3
54	0.008645	0.000019	1.467378	0.000049	0.001036	0.000044	0.280393	0.000012	-84.58	0.43	2960	2
61	0.008693	0.000029	1.467332	0.000102	0.001105	0.000025	0.280425	0.000016	-83.46	0.56	3601	2
63	0.008617	0.000013	1.467486	0.000074	0.000572	0.000014	0.280359	0.000021	-85.77	0.73	3613	2
66	0.008660	0.000010	1.467395	0.000048	0.000490	0.000005	0.280462	0.000012	-82.13	0.41	3639	8
67	0.008635	0.000012	1.467380	0.000050	0.000862	0.000012	0.281047	0.000010	-61.46	0.34	2856	7
70	0.008652	0.000017	1.467356	0.000045	0.000805	0.000019	0.281042	0.000013	-61.63	0.46	2862	7
72	0.008644	0.000016	1.467750	0.000160	0.000213	0.000002	0.280524	0.000037	-79.95	1.31	3636	5
77	0.008633	0.000010	1.467400	0.000054	0.000433	0.000020	0.280348	0.000013	-86.17	0.47	3805	3

a: Grain number corresponds to those for SHRIMP U-Th-Pb analysis - Table 1

b: Note Hf Heterogeneity within 2 spots of grain corresponding to 7/6 age

initial $^{176}Hf/^{177}Hf$	εHf(t)	2SD	CHUR mantle T(CHUR) Ga	T(CHUR) 2 -stage	Depleted mantle T(DM)1 Ga	T(DM) 2 -stage
		propagated errors including standards				
0.28024	-3.2	1.3	3.92	4.02	4.00	4.13
0.28043	0.4	0.9	3.63	3.61	3.75	3.81
0.28027	-6.6	0.7	3.88	4.08	3.96	4.18
0.28035	-1.4	1.7	3.76	3.80	3.86	3.96
0.28025	-0.1	1.8	3.90	3.91	3.99	4.04
0.28040	-1.7	1.1	3.68	3.73	3.80	3.91
0.28032	-0.4	1.2	3.80	3.81	3.90	3.97
0.28039	-0.9	0.9	3.69	3.71	3.80	3.89
0.28037	-1.5	0.8	3.72	3.76	3.83	3.93
0.28029	-1.7	1.9	3.84	3.89	3.93	4.03
0.28037	-2.6	0.7	3.72	3.80	3.83	3.96
0.28033	-3.9	0.9	3.78	3.90	3.88	4.04
0.28027	-0.6	0.8	3.87	3.89	3.96	4.03
0.28033	0.6	0.8	3.78	3.76	3.89	3.93
0.28095	2.5	1.3	2.84	2.77	3.08	3.15
0.28029	1.1	0.7	3.84	3.81	3.94	3.96
0.28027	0.6	0.8	3.86	3.85	3.96	4.00
0.28045	0.7	0.7	3.60	3.58	3.73	3.78
0.28035	-2.0	0.9	3.75	3.81	3.86	3.97
0.28033	-1.7	1.1	3.79	3.84	3.89	3.99
0.28028	-1.1	0.9	3.85	3.88	3.94	4.02
0.28034	-1.1	0.8	3.76	3.80	3.87	3.96
0.28039	-1.7	0.6	3.69	3.75	3.81	3.92
0.28070	-11.9	1.3	3.24	3.59	3.42	3.80

0.28032	-0.2	1.0	3.80	3.81	3.90	3.96
0.28037	-0.6	1.0	3.73	3.75	3.84	3.92
0.28071	-8.1	0.9	3.22	3.46	3.40	3.70
0.28097	-2.5	0.9	2.82	2.89	3.06	3.25
0.28045	-21.4	1.0	3.62	4.24	3.75	4.32
0.28098	1.3	0.8	2.80	2.76	3.04	3.14
0.28040	-2.1	0.7	3.68	3.74	3.80	3.92
0.28097	0.2	1.4	2.83	2.82	3.06	3.19
0.28037	-2.1	0.9	3.73	3.80	3.84	3.96
0.28028	0.9	0.9	3.85	3.83	3.95	3.98
0.28027	-0.6	0.8	3.87	3.89	3.96	4.03
0.28036	-1.5	0.7	3.74	3.79	3.85	3.95
0.28047	1.4	0.8	3.57	3.53	3.70	3.75
0.28035	-1.9	0.9	3.76	3.82	3.87	3.97
0.28099	2.6	0.9	2.79	2.71	3.03	3.10
0.28038	-2.0	0.8	3.71	3.77	3.82	3.94
0.28067	-13.1	0.6	3.28	3.66	3.45	3.86
0.28031	-1.8	0.8	3.81	3.87	3.91	4.01
0.28065	-15.8	0.9	3.31	3.77	3.48	3.95
0.28044	-1.1	0.8	3.62	3.66	3.75	3.85
0.28071	-11.6	1.3	3.22	3.57	3.40	3.78
0.28099	-0.5	1.0	2.79	2.81	3.04	3.18
0.28039	-0.3	1.0	3.70	3.71	3.81	3.89
0.28039	-0.9	1.0	3.69	3.71	3.80	3.89
0.28034	0.3	1.9	3.76	3.75	3.87	3.92
0.28034	0.4	1.8	3.76	3.75	3.87	3.92
0.28054	-17.7	0.9	3.49	4.00	3.64	4.12
0.28077	-12.9	1.0	3.15	3.51	3.34	3.74
0.28031	-2.1	1.1	3.82	3.88	3.92	4.02
0.28095	2.5	1.1	2.84	2.77	3.08	3.15
0.28036	-0.9	0.9	3.75	3.77	3.85	3.94

0.28103	1.3	1.1	2.73	2.69	2.98	3.09
0.28093	-1.6	1.1	2.89	2.93	3.11	3.28
0.28105	4.2	1.4	2.70	2.57	2.95	2.99
0.28100	-0.8	1.6	2.78	2.81	3.03	3.18
0.28038	-0.1	0.8	3.71	3.71	3.82	3.89
0.28037	-0.7	0.8	3.72	3.75	3.83	3.92
0.28090	-4.7	1.0	2.93	3.07	3.16	3.39
0.28049	-19.9	1.1	3.54	4.13	3.68	4.23
0.28103	4.6	1.1	2.72	2.58	2.97	3.00
0.28097	-0.3	1.0	2.82	2.83	3.07	3.20
0.28097	-1.2	1.0	2.82	2.85	3.06	3.22
0.28025	-0.7	0.9	3.90	3.92	3.99	4.05
0.28084	-14.2	1.4	3.03	3.44	3.24	3.69
0.28086	-6.2	0.8	2.99	3.17	3.20	3.47
0.28101	1.3	0.9	2.75	2.71	3.00	3.11
0.28100	-0.5	0.7	2.77	2.78	3.01	3.16
0.28094	-2.7	1.7	2.87	2.95	3.11	3.30
0.28097	-2.2	0.9	2.82	2.89	3.06	3.24
0.28095	-1.1	0.8	2.85	2.88	3.08	3.24
0.28101	1.6	1.1	2.76	2.72	3.01	3.11
0.28043	-22.6	0.7	3.63	4.30	3.75	4.37
0.28100	1.0	0.8	2.78	2.75	3.02	3.13
0.28099	0.1	1.5	2.78	2.78	3.03	3.16
0.28100	1.7	1.1	2.77	2.72	3.02	3.11
0.28038	-0.7	0.9	3.71	3.73	3.83	3.90
0.28046	-22.8	0.9	3.61	4.27	3.74	4.34
0.28027	-0.3	1.0	3.86	3.87	3.95	4.02
0.28097	2.2	0.9	2.82	2.75	3.06	3.14
0.28103	-0.1	0.9	2.73	2.74	2.98	3.13
0.28099	2.7	0.8	2.79	2.71	3.03	3.10
0.28100	0.6	0.8	2.78	2.76	3.02	3.14
0.28100	1.0	0.8	2.77	2.74	3.02	3.13
0.28089	0.1	1.4	2.95	2.94	3.18	3.29

0.28041	-0.8	1.3	3.67	3.69	3.78	3.87
0.28104	2.7	1.3	2.71	2.63	2.96	3.04
0.28098	0.3	0.7	2.81	2.80	3.05	3.18
0.28038	-23.9	1.1	3.72	4.42	3.83	4.46
0.28096	0.4	0.8	2.83	2.82	3.07	3.19
0.28047	-12.5	0.9	3.57	3.95	3.70	4.08
0.28045	1.1	1.0	3.60	3.57	3.73	3.78
0.28035	-2.5	0.7	3.75	3.82	3.85	3.98
0.28023	-5.9	0.8	3.94	4.11	4.02	4.21
0.28015	-8.5	0.9	4.05	4.31	4.11	4.36
0.28032	-2.2	0.8	3.79	3.86	3.89	4.01
0.28033	1.5	1.3	3.79	3.74	3.89	3.91
0.28030	-0.5	0.8	3.82	3.84	3.92	3.99
0.28032	0.1	0.7	3.80	3.80	3.90	3.96
0.28046	-11.3	1.6	3.60	3.94	3.73	4.07
0.28030	0.1	0.9	3.82	3.82	3.92	3.97
0.28100	0.5	0.9	2.78	2.77	3.02	3.15
0.28026	-1.9	1.0	3.88	3.94	3.97	4.07
0.28036	-3.4	1.2	3.74	3.84	3.85	4.00
0.28098	-0.4	0.8	2.81	2.82	3.05	3.19
0.28098	-0.3	0.6	2.81	2.82	3.05	3.19
0.28028	0.1	0.9	3.85	3.85	3.95	4.00
0.28038	-2.9	1.0	3.71	3.80	3.82	3.96
0.28028	0.0	1.1	3.86	3.86	3.95	4.00
0.28046	-7.6	1.1	3.60	3.82	3.73	3.98
0.28098	0.8	0.8	2.81	2.78	3.05	3.16
0.28040	-0.7	0.8	3.67	3.69	3.79	3.88
0.28028	-0.4	0.9	3.86	3.87	3.95	4.02
0.28044	1.9	1.0	3.61	3.56	3.74	3.77
0.28074	-10.6	0.7	3.18	3.49	3.36	3.72
0.28095	0.3	1.4	2.85	2.85	3.10	3.21

0.28031	0.5	0.8	3.81	3.80	3.91	3.96
0.28101	-4.2	0.9	2.76	2.89	3.01	3.25
0.28033	-19.3	1.0	3.80	4.36	3.90	4.41
0.28035	-3.7	1.2	3.76	3.87	3.87	4.01
0.28032	-4.4	1.5	3.80	3.93	3.90	4.07
0.28043	0.1	0.9	3.64	3.63	3.76	3.83
0.28100	1.9	0.8	2.77	2.72	3.02	3.11
0.28100	2.0	1.0	2.78	2.72	3.02	3.11
0.28051	2.9	2.6	3.51	3.42	3.65	3.66
0.28032	0.1	1.0	3.80	3.80	3.90	3.96